Bi-directional Thulium-doped Fiber Lasers

(双方向ツリウム添加ファイバレーザ)

THE UNIVERSITY OF TOKYO

Hongbo Jiang

Supervisor: Prof. Sze Yun Set

Electrical Engineering and Information Systems

University of Tokyo

July 2018

Acknowledgements

Firstly, I would like to express my sincere gratitude to my advisor Prof. Set for the continuous support of my master study and related research, for his patience, motivation, positive spirit, and most precious, his genius brain and immense knowledge. His guidance helped me in all the time of research and writing of this master thesis. I could not have imagined having a better advisor and mentor for my master study. Besides my advisor, I would like to thank Prof. Shinji Yamashita for his insightful comments on experiment design, and unexpected phenomenon analysis. I would like to thank my mentor Dr. Yu Wang, the man who enlighten me the first glance of research, I couldn't even make my life in Japan without his continuous guidance. I would like to thank Dr. Andrew Malouf and Dr. Wenqi Zhang for their help when I was in Adelaide alone, all because of them, I spent an incredible time there.

My sincere thanks also goes to Ms. N. Tomiyoshi, who is the secretary of yamashita-set lab, for her generous help and her understanding on the language difficulties even this always gets her into trouble.

I thank all my fellow lab mates, especially Dr. Goran Kovacevic, Dr. Takuma Shirahata, Mr. Pengtao Yuan, for the stimulating discussions, for the sleepless nights we were working together before deadlines, and for all the fun we have had in the past two years. Also I thank all my friends in University of Tokyo and BUPT. In particular, I am grateful to Ms. Shoko Yokokawa and Mr. Zihao Zhao for working together with me.

Last but not the least, I would like to thank my family: my parents for supporting me spiritually and financially. And to my beloved, Ms. Kaiyue Liu, for giving me encouragement and fully trust during this period.

Abstract

The research on soliton fiber lasers operated in 2 μm have been discussed with great interest in several years. Lasers in 2 μm wavelength region have unique properties like significant low damage to retina, moderate absorption of water and CO_2. Meanwhile, ultrashort pulses at 2 μm generated by mode-locked Thulium-doped fiber lasers could be used for surgery, time of flight (TOF) technology and optical frequency comb (OFC) for gas detection. Conventional mode-locked Thulium doped fiber lasers realized with different methods such as semiconductor saturable absorber mirrors, nonlinear polarization evolution, and pump/loss modulation, regardless of their inherent weaknesses like high cost, low robustness and low repetition rate, all the conventional mode-locked Thulium doped fiber lasers have a common feature that an optical isolator is inserted into cavity, which can regulate the pulse trains in single direction and improve the performance. However, the existence of optical isolator in laser resonator will block another direction, not just inside the cavity. The mode-locked fiber lasers have been proved to work as a seed source for dual-comb spectroscopy, which utilizes the beating signal generated by two ultrashort pulse trains with slightly different repetition rates to obtain the entire sample spectrogram without the need of optical spectrum analyzer. Therefore, more investigation in 2 μm isolation-free or bi-directional operation mode are needed. Besides, the isolation-free ring structure enables the self-sweeping phenomenon in the cavity, the sweeping range can be extended to 15 nm, and it can be categorized as laser mode instability and has the potential application as sweeping laser source. Moreover, a residual polarization dependent loss induced mode locking method is demonstrated, the possible physical mechanism is discussed. The purpose of this thesis is to study passive mode-locking methods and bi-directional operation behavior in thulium doped fiber laser, the wavelength self-sweeping fiber laser induced by spatial hole burning and passive mode locking method induced by residual polarization dependent loss are demonstrated for the first time.

Table of contents

List of figures

List of tables

Chapter 1

Research Background

1.1 What is the Superiority of 2 μm?

2 μm, which is also called "eye-safe wavelength", has attracted great interest in academia and industry because its unique properties in water absorption, gas detection and other areas. Some of the properties of 2 μm and the potential applications resulting from these properties will be demonstrated in this section.

Carbon dioxide (CO_2) is the main greenhouse gas that has a significant impact on Earth's climate. Therefore, detecting CO_2sources is a top priority. However, The CO_2 exists on Earth in different types and has complicated interactions with different substance, which makes the detection CO_2 difficult. Great research efforts by world leading research group like NASA has been made during the last twenty years. All these CO_2 sensing and monitoring projects issued by NASA were accomplished by using 2 μm lasers because the excellent absorption features at this wavelength region. For instance, a 2 μm laser could be tuned over or stabilized to CO_2 or H_2O vapor lines. The significant CO_2 absorption feature is demonstrated in Fig 1.1. Besides, a brief conclusion of CO_2 detection missions issued by NASA is shown in Table 1.1. Moreover, the significant absorption of CO_2 is not the only reason that make this wavelength so attractive, another substance which has irreplaceable absorption property is water vapor, which is demonstrated in Fig reffig:H2O. This specific absorption property attributes 2 μm to so called "eye-safe" wavelength region. Because of the extremely extension of laser applications such as remote sensing and laser radar, eye safety could be a big problem which directly promote the use of those lasers lasing beyond 1.4 μm. The maximum permissible eye exposures are pretty much higher than other wavelength region. The relationship between eye safety and laser operation should be divided into two parts. Firstly, the general definition of "eye-safe" is that the light should be totally absorbed before it reaches retina, the sensing part of eye, the water in corneal tissue blocks the light

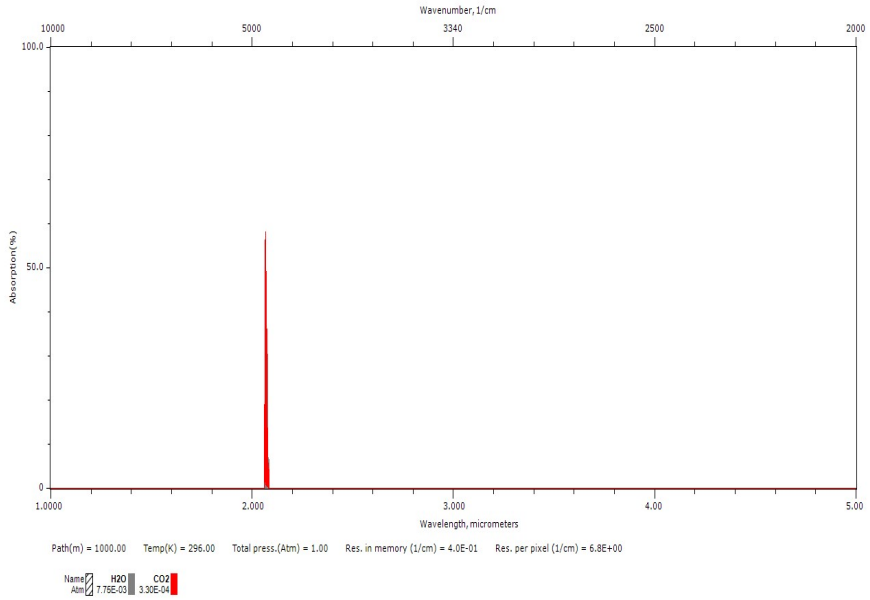

Fig. 1.1 CO_2 absorption spectrum from 1 µm to 5 µm

beyond 1.4 µm, this prevents the direct damage to retina. However, only the requirement on wavelength is not reliable, if the light absorption in corneal is too high, the heat caused by the water absorption, which brings damage to eyes as well. And that is the reason why the modest absorption in water makes lasers at 2 µm become outstanding and more and more important.

1.2 Why We Need Mode-Locked Fiber Laser?

The history of laser has passed through decades since the first laser was demonstrated by 1960s' and the invention of lasers had impacted human being's society significantly. But here we want to highlight one type of lasers: mode-locked lasers. Mode-locked lasers have been used in different fields like medical devices, material processing, remote sensing, and free-space optical communications because of its unique and excellent properties in spatial and spectral domain.

Generally, a mode-locked laser is a laser operated in mode locking mode which forces all the longitudinal mode in laser resonator phase locked with each other in order to generate optical ultrashort pulses with duration from 10 fs to 100 ps. These femtosecond or picosecond lasers not only inherit the advantages of basic lasers, but also have outstanding advantages

Table 1.1 General and specific attributes of 2 µm lasers for CO_2 active remote sensing

2 µm lasers attributes	Carbon Dioxide Detection
Low Atmospheric Extinction	Enhance CO_2 measurement sensitivity
High Pulse Energy	Enhance CO_2 measurement sensitivity and/or relax detection requirements
High Pulse Rate	Allows more averaging that enhance CO_2 measurement sensitivity by reducing random error
Excellent Beam Quality	Reduce CO_2 measurent systematic errors
Wavelength Tunability and Locking	Differential absorption lidar (DIAL) requires on-line tuning across CO_2 absorption at off-line
Multi-Pulse Capability	Permits single or double species measurements with single transmitter

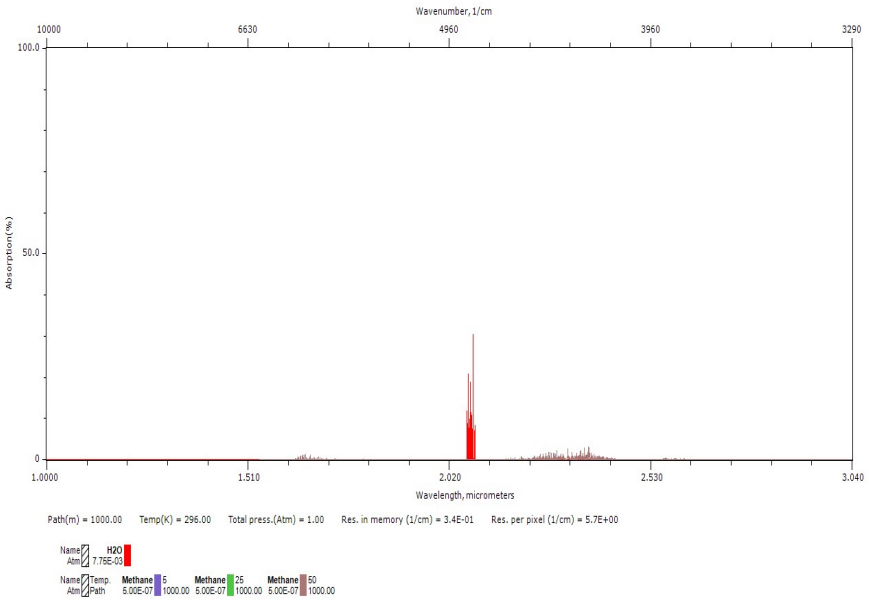

Fig. 1.2 H_2O absorption spectrum from 1 µm to 5 µm

in providing ultrashort pulses, high peak power, variable repetition rate from Megahertz to Gigahertz depending on the needs of various applications.

Similar to normal lasers, the mode locked lasers also have the different platform like mode-locked solid state lasers and fiber lasers. Even though today's main platform of mode-locked lasers is still governed by solid state lasers, especially mode-locked Ti-sapphire lasers because these lasers can offer ultrashort pulse duration, high pulse energy and relatively high repetition rate at the same time, which are attractive for various fields. However, all these advantages of mode-locked solid state lasers are counteracted by the inherent short comes, including huge size, high cost, and complex adjustment and maintenance. Different from mode-locked solid state lasers, mode-locked fiber lasers have excellent properties on cost, flexible and simple implementation.

Such great advantages of mode-locked lasers, or, be more specific, mode-locked fiber lasers have enabled a wide range of applications. For instance, active gas sensing is one of the promising applications with mode-locked fiber laser involved as we have mentioned in the previous section (see Section 1.1). In addition, mode-locked fiber lasers can provide precise light control and high pulse energy, so that we can locate the pulse on the focus of infection instead of peripheral tissue, which fulfill the need of surgical applications. What's more, mode-locked fiber laser for LiDAR is also a hot topic at the moment and has a promising future.

1.3 Purpose and Organization of This Thesis

Mode-locked fiber lasers have been studied over two decades, various implementation and laser cavity design comes out one after the other. Although their configuration or the purpose of design might be various, one of the common principle that makes most of mode-locked fiber lasers in common with each other is the single directional running, in other words, for most mode-locked fiber lasers, we have to force the light propagate in the direction we preferred in order to generate the stable, constant output. For instance, the lack of single direction step will attribute to reflection and interference, which affects the output of cavity then undermines the performance of laser accordingly. In the ring cavity configuration, we always insert a optical isolator in cavity to force the light propagate in either clockwise (CW) or counter-clockwise (CCW) direction, as we mentioned before. However, the contrary to popular belief, a type of so called "bi-directional" mode-locked fiber lasers has entered the researcher's attention. Differ of conventional mode-locked fiber lasers which operated in single directional, these lasers are operated in counter-circulating direction in a quasi-constant mode. The conventional mode-locked fiber lasers generate ultrashort pulse in

single directional while these bi-directional mode-locked fiber lasers generate two opposite ultrashort pulse trains simultaneously with high coherence and simple configuration. The invention of bi-directional fiber lasers opened alternative for precise rotation sensing and gas spectroscopy since the simultaneous produced, counter-circulating pulse trains in the same cavity have highly coherence, locked difference in repetition rate and quasi-constant beating signal for sensing use which generated by the opposite outputs. To date, bi-directional mode-locked fiber lasers have been demonstrated by many groups even though the intrinsic principle of separation of repetition rate is still blurry.

The purpose of this thesis is to study the behavior of the 2 μm bi-directional fiber laser, the physical mechanism for center wavelength separation and unbalanced output, carbon nanotube is chosen for initiating the soliton generation. Moreover, wavelength self-sweeping attributed by the absence of optical isolator in the cavity are demonstrated, the physical mechanism and potential application are discussed. A new passively mode locking method is demonstrated and the physical mechanism is discussed. as well.

Chapter 2 illustrates the concepts and fundamentals of mode locking theory, including different mode locking methods, pulse operation regimes and mathematical analyze of soliton wave's behavior in fiber lasers. Chapter 3 introduces fundamentals of dual-comb spectroscopy, explain the connection between dual-comb spectroscopy and bi-directional mode-locked fiber lasers. Chapter 4 describes the 2 μm in detail including configuration, novel points from previous research, results analysis such as the physical mechanism of repetition rate separation. New phenomenon from the isolation free ring cavity–wavelength self-sweeping is depicted in Chapter 5. Chapter 6 is s summary and a brief introduction on passively mode locking phenomenon induced by bending of single mode fiber coils with small radius or a patch cord with working wavelength of 1060 nm.

Chapter 2

Fundamentals of Mode-locked Fiber Lasers

In this chapter, the concepts and fundamentals of mode locking theory including mode locking, different mode locking methods, saturable absorber, soliton theory, fiber coils polarization controller and mathematical analysis will be introduced.

2.1 Concept of Mode Locking

Mode locking is a group of methods to obtain ultrashort pulses from lasers. The origin of the term mode locking is from a specific description in frequency domain as shown in Fig 2.1. There are a large number of longitudinal modes simultaneously exist in the laser resonator. The number of longitudinal modes is rely on the gain bandwidth of a gain medium, the separation between neighboring modes δv is depend on the optical length of the laser cavity L_c. The relationship between is given by

$$\Delta v = \frac{c}{L_c} \tag{2.1}$$

and the total optical field of longitudinal modes in resonator is

$$E(t) = \sum_{m=-q}^{q} E_m exp(i\phi_m - i\omega_m t) \tag{2.2}$$

where E_m, ϕ_m and ω_m represent the amplitude, phase and oscillation frequency of the m-th longitudinal mode. Mode locking situation is formed when the phase relationship between longitudinal modes is fixed, the larger the number of frequency modes involved,

the shorter can be the duration of the generated pulses, the fixed phase relationship should follow: $\phi_q - \phi_{q-1} = constant$ Besides, the formula 2.2 can be simplified as follow if we all longitudinal modes have the equal amplitude

$$|E(t)|^2 = \frac{sin^2(N\pi\Delta\nu t + \phi_{constant/2})}{sin^2(N\pi\Delta\nu t + \phi_{constant/2})} E_0^2 \tag{2.3}$$

One can easily find from (2.3) that the peak power of total longitudinal mode is N^2 times of only mode. What is more important is that the pulse width is inversely proportional to the optical spectral bandwidth in frequency domain according to Fourier transformation, or the number of phase-locked longitudinal modes, $1/(\Delta\nu N)$ approximately. If we look at the peak point at regular temporal positions from the total power of the signal, the electric fields of all longitudinal modes contribute to a maximum of the total field strength in time domain, which is illustrated in Fig. 2.2 and this is the significant property of mode locking theory which enables the mode-locked lasers outstanding from continuous wave lasers. In summary, one of the important aspect for the formation of short pulse is that they must be a "locked" phase relationship between longitudinal modes. Once the "locked" relationship is destroyed and become random phase relationship, then the laser output become continuous wave whose average optical power is shown in Fig. 2.2

2.2 Different Mode Locking Methods

Mode locking teniques can be classified into three basic categories: active, passive and hybrid.

For active mode locking, an active device driven by an external signal is required to modulate the loss inside the cavity. Either a bulk modulator or an integrated electro-optic $LiNbO_3$ modulator can be used for active mode locking as long as the modulation frequency match with the free-spectral range (FSR) of the cavity. The typical configuration of active mode-locked fiber laser and the pulse formation by using active mode locking is shown in Fig. The loss of the cavity is modulated periodically and the short pulse is formed at the temporal positions that having minimum loss in the cavity. Active mode locking has the advantage of high repetition rate since the modulate frequency can work at a rational harmonic of the fundamental frequency. The implementation of modulator enable mode-locked fiber lasers produce ultrashort pulses at speed of GHz, which is the most significant superiority of active mode locking technique and is really important in high-speed communications transmission

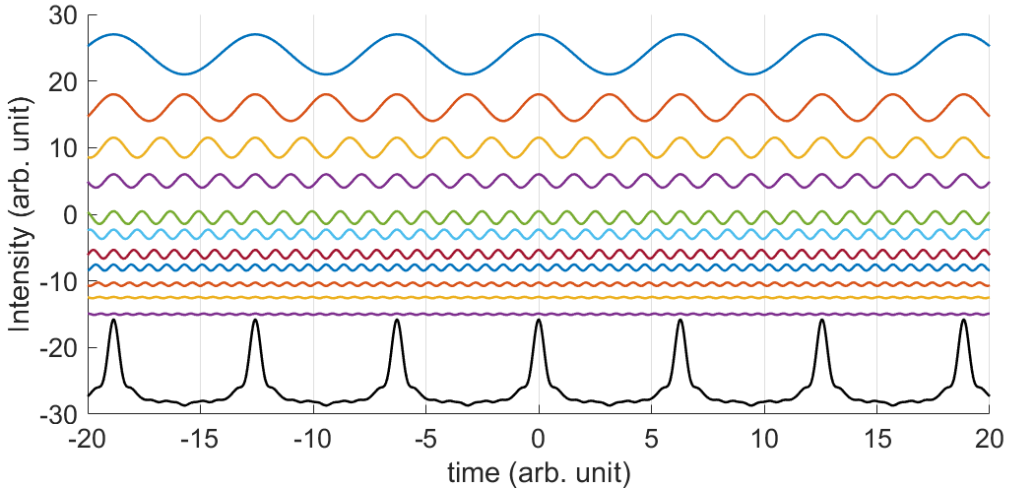

Fig. 2.1 Synthesis of a periodic pulse train (black curve) by adding ten oscillations with different frquencies (curves in different color). The phase-fixed points like t=0 enable the formation of short pulse

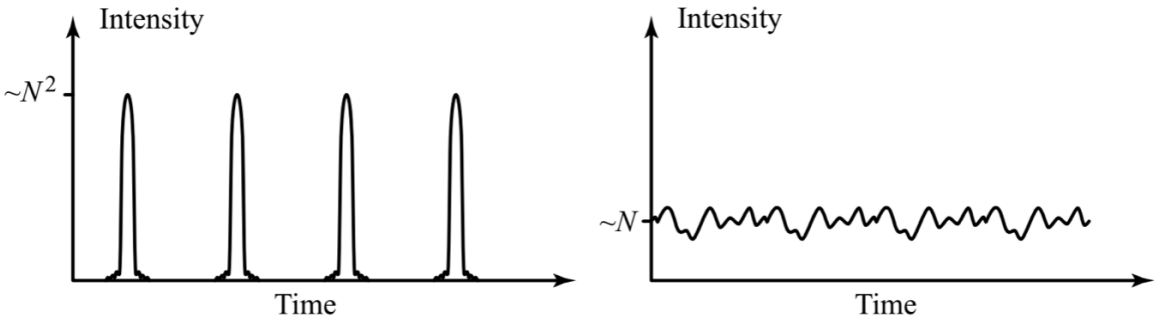

Fig. 2.2 Output intensity comparison between continuous wave and mode locking [1].

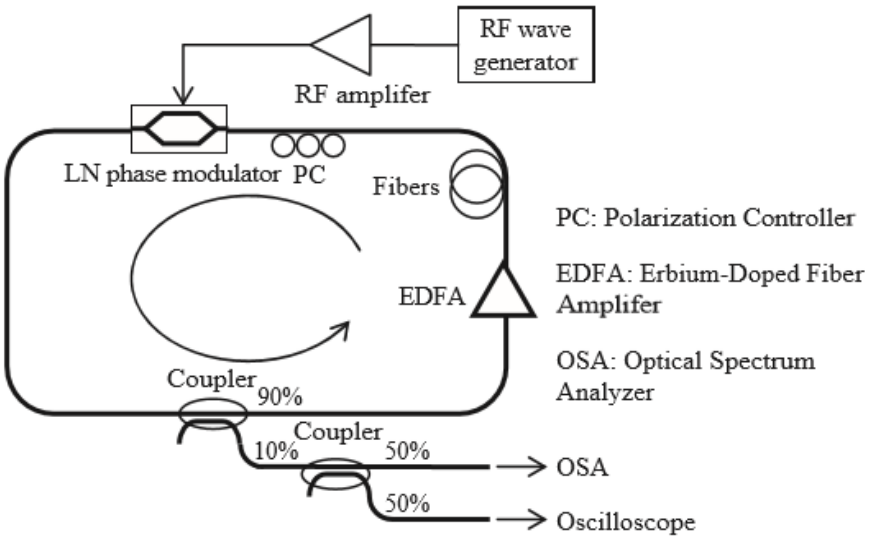

Fig. 2.3 Experiment setup of the active frequency modulation mode-locked fiber laser [2].

system. However, a stable pulse train in a long term is required and challenging at the same time. Because mode-locked fiber laser using active mode locking method can be easily affected by the fundamental frequency drifting, polarization states change and DC shift of the modulator [13, 14] which possibly make the modulation frequency is not equal to a rational harmonic frequency any more, it is difficult for an active mode locking to maintain a stable output in the long term.

Passive mode-locked fiber lasers achieve mode locking by using a saturable absorber without using any external signal. Pulse formation and a group of typical configurations of passive mode-locked fiber laser are shown in Fig. 2.4 A saturable absorber introduces an intensity-dependent discrimination where the peak of pulse experience a strongly saturate curve while the wings of the pulse which have low intensity experience higher loss during pulse shaping. The pulse is shortened to a comparable level of the gain medium bandwidth. There are different types saturable absorber have been used in passive mode locking over decades such as nonlinear polarization rotation (NPR) [15–17],nonlinear optical loop mirrors (NOLM) [18], nonlinear amplifying loop mirrors (NALM) [19],semiconductor saturable absorber mirrors (SESAM) [20],carbon nanotube/graphene [21–23],Molybdenum disulfide (MoS_2) [24].The width of pulse generated from passive mode-locked fiber lasers is very narrow and can be the order of 10 fs [25–27]. A tipical NPR structure is shown in Fig. 2.4c. The linearly polarized light is transformed into elliptically polarized light, pass through the medium then transform into linear polarization again. When the elliptical light rotates with the Kerr effect while the angle of rotation is proportional to the light intensity. In all-fibred

structure, two polarization controller sandwich on polarizing isolator. NPR is well-known for its simple configuration and capability of responding at femtosecond timescales, however, it is easily affected by environmental fluctuation. Mode locking can be achieved by NOLM or NALM as well which is ascribed by the different nonlinear phase shifts of fields since the intensity of different direction has different intensity. This structure is ia to achieve but it is difficult to obtain high repetition rate since the fiber coils must be inserted in the cavity. SESAM is a saturable absorber which takes advantage of large modulation depth. SESAM has significant drawbacks compared with other saturable absorber since the long recovery time and expensive cost. There is another type of saturable absorber made up of CNT/graphene, CNT is definite outstanding saturable absorber because of its wide absorption range, ultrashort recovery time, high optical damage threshold, and good compactness. Graphene has a frequency independent optical inter band transitions which enables it become a novel saturable absorber suitable from the visible to near-infrared region. Besides, a typical ring cavity mode-locked fiber laser initiates more easily [28, 29]. Even though passive mode locking method have such great advantages that can easily generate extremely ultrashort pulses, the repetition rate of pulse train generated from passive mode-locked fiber lasers is limited at the order of 100MHz. The reason for repetition rate limitation is due to the fundamental frequency which determined by the cavity length L_c.

Considering the superiority and drawbacks of passive and active mode locking, a promising technique that overcome the those drawbacks and succeed the advantages from both mode locking method is hybrid mode locking [30]. The mechanism of passive mode locking is used for further pulse shaping, MZ modulator is used for create high repetition rate. The combination of passive and active mode locking has been used to generate pulse train with the width order of 100fs at high repetition rate with the order of GHz [31]. Besides, we can also combine two different passive mode locking methods. A slow saturable absorber like carbon nanotube for initiating mode-locking and a fast saturable absorber like NPR for further pulse shaping. For instance, The configuration combine CNT with NOLM has been reported for self-starting recently [32].

2.3 Mode Locking Opreation Mode

To obtain the propagation behavior of optical pulse in a nonlinear guided medium such as optical fiber, Maxwell's equations are employed to derive the nonlinear wave evolution equation as follows [33]:

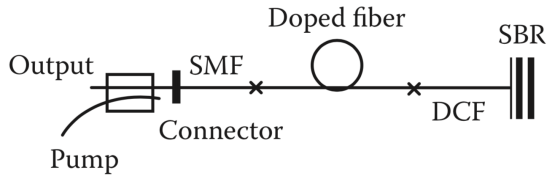

(a) Linear cavity configuration passive mode locking method

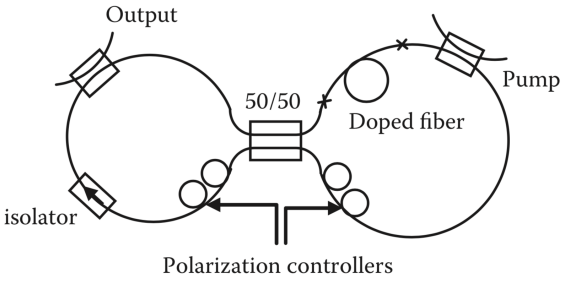

(b) Passive mode locking method with a configuration based on nonlinear fiber loop mirror

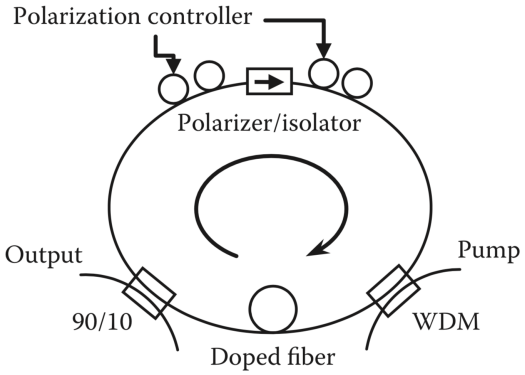

(c) Passive mode locking with a ring configuration based on nonlinear polarization rotation

Fig. 2.4 Collection of several kinds of passive mode locking method, picture from [2].

$$\nabla \times \nabla \times \vec{E} + \frac{1}{c^2}\frac{\partial^2 \vec{E}}{\partial t^2} = -\mu_0 \frac{\partial^2 \vec{P}}{\partial t^2} \tag{2.4}$$

where $\vec{E}$, mu_0 and c are, the electric field vector, the vacuum permeability, and the speed of light respectively. Since the $\nabla \cdot \vec{E} = 0$ for dielectric materials and the vector indentity $\nabla \times \nabla \times \vec{E} = \nabla(\nabla \cdot \vec{E}) - \nabla^2 \vec{E}$, 2.4 can be expresses as

$$\nabla^2 \vec{E} - \frac{1}{c^2}\frac{\partial^2 \vec{E}}{\partial t^2} = \mu_0 (\frac{\partial^2 \vec{P_L}}{\partial t^2} + \frac{\partial^2 \vec{P_{NL}}}{\partial t^2}) \tag{2.5}$$

$\vec{P_L}$ and $\vec{P_{NL}}$ are linear and nonlinear parts of polarization vector $\vec{P}$, the form of $\vec{P}$ and other related derivation are not explained here. The famous and widely used equation – nonlinear Schrödinger equation, which plays a key role in descripting optical pulse propagation behavior. It can be derived from wave equation(2.5) by steps:

$$\frac{\partial A(z,t)}{\partial z} + \frac{\alpha}{2}A(z,t) - j\sum_{n=1}^{\infty}\frac{j^n \beta_n}{n!}\frac{\partial^n A(z,t)}{\partial t^n} = j\gamma(1 + \frac{j}{\omega_0}\frac{\partial}{\partial t}) \times A(z,t)\int_{-\infty}^{+\infty} R(t')|A(z,t-t')|^2 dt' \tag{2.6}$$

where $A(z,t)$ is the slowly varying complex envelope, γ is nonlinear coefficient and $R(t)$ is the nonlinear response function. The equation 2.6 cna be further simplified if we use the following regulation :

1. Optical pulse propagating in medium is larger than100 fs.
2. The high-order nonlinear effect including Raman scattering and self-steepening can be neglected if pulse width is of the order of picosecond.
3. propagation constant β only includes the group velocity dispersion β_2
4. Regrad attenuation factor as zero.

then the simplified result is a one of the most popular equation which is empolyed to explain the opitcal pulse propagation behavior in ninlinear dispersive medium like optical fiber:

$$\frac{\partial A}{\partial z} + \frac{j\beta_2}{2}\frac{\partial^2 A}{\partial \tau^2} = i\gamma|A|^2 A \tag{2.7}$$

By using the following variables transformation,

$$\zeta = z/L_D, T = \tau/\tau_0, u = \sqrt{\gamma L_D} A \tag{2.8}$$

where τ_0 is taken to be width of iniaite pulse and L_D is the length of dispersion. NLSE 2.7 can be normalized as

$$j\frac{\partial u}{\partial Z} - \frac{s}{2}\frac{\partial^2 u}{\partial \tau^2} \pm |u|^2 u = 0 \tag{2.9}$$

The pulse opreation regime is depend on the sign of the group velocity dispersion β_2. If the total dispersion in the cavity is anomalous, then soliton pulses are generated. In case of anomalous group velocity dispersion, the most interesting solution of 2.7 is the formation of fundamental soliton:

$$u(\zeta, \tau) = sech(\tau) exp(j\zeta/2) \tag{2.10}$$

where $\zeta = z/L_D$ and $u = \sqrt{\gamma L_D} A$. When the input is given as $u(0, \tau) = sech(\tau)$, Solution 2.10 can be transferred into real units as

$$A(0, T) = \sqrt{P_0} sech(\frac{T}{T_0}) = (\frac{|\beta_2|}{\gamma T_0^2})^{1/2} sech(\frac{T}{T_0}) \tag{2.11}$$

Solution 2.11 indicates that fi there is a hyperbolic-secant pulse with peak power P_0 can propagate unistorted change in temporal and spectral shapes. This key feature results from the balances between GVD and SPM effect. It is worth to note that the soliton pulse is only stable for a given peak power, higher peak power leads to multiple soliton excited in the cavity.

Thanks to the technique of dispersion management [34], The pulse-like, periodic solutions formed which usually referred as stretched pulse or dispersion-managed soliton [33] since the laser is made of two types of fibers enable the net dispersion to be near zero. Stretched pulse have a Gaussian shape spectral shape without Kelly sidebands. The stretched pulse enables the high peak power and high pulse energy.

When the cavity dispersion is in normal dispersion, another approach of ultrashort pulse generation is achieved because of periodically amplified and losses. The pulse is formed unlike the conventional soliton with anomalous dispersion, the nonlinearity is not only

balanced by the dispersion, dissipative processes such as gain and losses contribute to the balance process as well [35]. The spectrum of dissipative pulses always has steep edges and the shape of spectrum shape of dissipative pulses is flexible depends on cavity design such as nonlinearity, dispersion and bandwidth [36].Due to periodic perturbations during round-trip of solitons, they dissipate the energy to keep stabilization. A frequency chirping can help to maintain the stable states in fiber system, and it explains why dissipative solitons are chirped inside the cavity.

2.4 Q-switching, Self-starting and Multiple-pulsing

Historical interrogation of saturable absorbers has shown that various kinds of saturable absorber can be used for mode locking. During the setup of passive mode-locked laser with a saturable absorber, one should think about the engineering strategy including Q-switching instability, self-starting and multiple-pulsing which may have different impact on the laser performance.

Let's introduce Q-switching instability at first. Normally, continuous wave mode-locking as shown in Fig. 2.5 produces a regular pulse train which is exactly desired mode for most of passive mode-locked lasers. However, mode-locked laser can exhibit Q-switching or even operate in Q-switched mode locking regime. It is important for most of stable passively mode-locked lasers that operating in cw mode-locking regime without Q-switching instabilities. Passively mode-locked lasers using saturable absorber with long upper-state lifetimes have a strong tendency to Q-switching regime [37]. Many works have been reported that appropriate parameters can control the dynamics inside the cavity so that the Q-switching can be suppressed [38, 39]. The criterion for cw mode locking against Q-switching instability has been derived following the Master Equation approach. Assuming that the saturable absorber saturates with pulse energy and recovers fully before the next pulse. Therefore, the Q-switching instability can be prevented if

$$E_p \frac{dR(E_p)}{dE_p}|_{E_p} < \gamma \frac{T_R}{\tau_l} \tag{2.12}$$

Where E_p is the operational pulse fluence, $\frac{dR(E_p)}{dE_p}|_{E_p}$ is the slope of the saturation curve $\gamma = 1 + P/P_{sat,L}$, P is the average intracavity power and $P_{sat,L}$ is the saturated power of the active medium. T_R is the round trip time and τ_l is the upper-state lifetime of the gain medium. The detail derivation of Equation 2.12 is not presented but an intuitive physical interpretation of it can be explained as follows: On the time scale corresponding to the upper state-lifetime

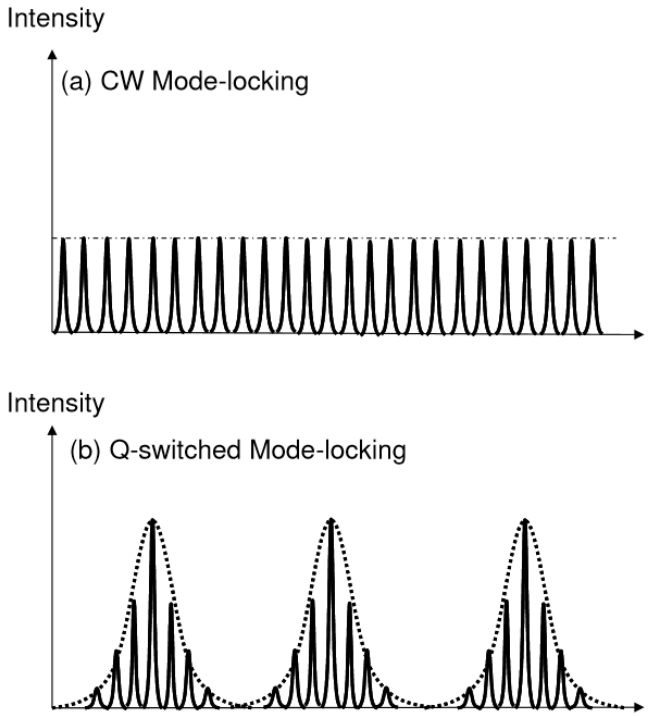

Fig. 2.5 Pulse trains of a stable continuous wave mode locking (a) and Q-switched mode locking (b).

of the laser, the left side of Equation 2.12 describes the fluctuation in pulse energy, where the right side of Equation 2.12 shows the declination of gain results from gain saturation caused by pulse energy increasing. If the gain saturation can suppress the growth of pulse energy, the Q-switching instability can be avoided. Otherwise, the amplitude modulation to pulse train appears as shown in Figure 2.5.

In practice, gain medium should be fully saturated by decrease the length of active fiber or keep increasing the pump power. Although the physical mechanism have not been fully understood, some theoretical studies have been reported during the past twenty years. [40–42]

Self-starting is another common engineering strategy which is highly dependent on the whole design of the cavity while Q-switching's criterion is dominated by the design of saturable absorber. In contrast to Q-switching, self-starting is much more complicated and related to the dispersion of cavity, stability of laser, parasitic reflections in the cavity, pump level, gain cross section and many others.

Ideally, for homogeneously broadened laser without spatial hole burning and absence of saturable absorber, single longitudinal mode is supported in the cavity which is at the center of the gain spectrum and leads to the saturation of the gain. When a saturable absorber is inserted into the cavity, many longitudinal modes are supported and phase locked, the

effect of saturable absorption decides the mode-locked lasers could automatically start mode locking without external interventions or not. In practice, a criterion for saturable absorber is that the saturation fluency should be as low as possible and the modulation depth should be as high as possible without resulting in Q-switching instabilities.

The passive mode-locked lasers commonly experience multiple pulsing under strong pumping. For the generation of high-energy pulses, multiple pulsing limits the generation of high energy pulse since the multiple pulsing is favored in the cavity [43]. The sophisticated physical explanation of multiple pulsing is not concluded yet but when there is reverse saturable absorption or two-photon absorption occurring in the saturable absorber at high pump level, the laser favors multiple pulses instead of high energy single pulse.

2.5 Principle of Fiber Loop-based Polarization Control

Ideally, the single-mode fiber we used can support two orthogonally polarized mode, HE_{11x} and HE_{11y}, with same phase velocity(propagation constant $\beta_x = \beta_y$). However, single mode fiber are not perfectly circularly symmetric practically, which causes the different phase and group velocities. Besides, environmental factors including arbitrary bend and twist destroy the degeneracy between two modes and produce the birefringence accordingly.

In order to overcome the polarization status fluctuations and remain the all fiber structure we can introduce a fiber loop-based polarization controller to manipulate the polarization status in the cavity on purpose. The change of refractive index in x axis and y axis:

$$\Delta n_x = \frac{n^3}{4}\left(p_{11} - 2\rho p_{12}\right)\left(\frac{a}{R}\right)^2 \tag{2.13}$$

$$\Delta n_y = \frac{n^3}{4}\left(p_{11} - \rho p_{12} - \rho p_{12}\right)\left(\frac{a}{R}\right)^2 \tag{2.14}$$

where a is the core radius of single mode fiber, R is the radius of curvature, p_{ij} represent the elasto-optical coefficient of fused fiber and ρ is Poisson's ratio. Therefore:

$$|\delta n| = \left|\Delta n_x - \Delta n_y\right| = 0.133\left(\frac{a}{R}\right)^2 \tag{2.15}$$

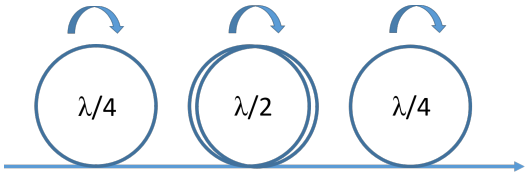

(a) Polarization controller using multiple coiled fiber.

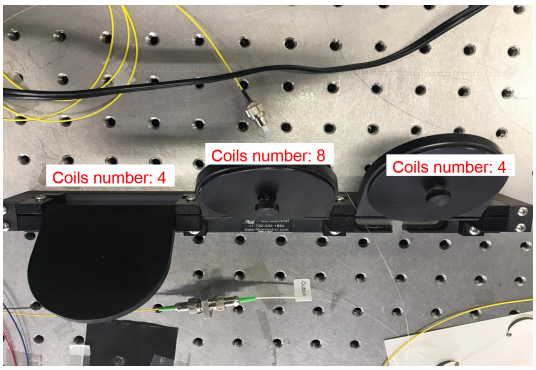

(b) A fiber coils-based polarization controller in yamashita-set lab.

Fig. 2.6 Fiber coils-based polarization controller

From 2.15, the fiber loop in specific radius can provide birefringence and work as wave plate, if the radius of curvature R and loop number N have the following relationship with wavelength λ :

$$|\delta n| 2\pi NR = \frac{\lambda}{m} \tag{2.16}$$

For instance, assuming that our fiber laser is working in 2 µm, we ring the single mode fiber that has the cladding radius of 62.5 µm to fiber loops that have a radius $R = 20.6mm$, when the number of loop is four, the structure becomes a $\lambda/4$ wave plate while the number of loop is eight, it equals a $\lambda/2$ wave plate. The controlling principle in fiber loop is similar to the free space using wave plates, the configuration is shown in Fig 2.6a, the second fiber coils acting as a Half-Wave Plate (HWP) is sandwiched between the first and third fiber coils which acting as two Quarter-Wave Plates (QWP) and the retardation planes are free to rotate around the optical beam. The first fiber coils transfer any arbitrary polarization state from input port into a linear polarization. The second fiber coils rotate the linear polarization to a specified angle so that the third fiber coils can convert the angle-specified linear polarization to any polarization state we want. A fiber coils-based polarization controller in yamashita-set lab is shown in Fig 2.6b.

2.6 Super Continuum Generation

Even though ultrashort pulses have plenty of advantages such as short pulse duration, high peak power and high repetition rate, the typical ultrashort pulse in optical spectra is extremely limited by the gain bandwidth. The wavelength of ultrashort laser is restricted in 10 nm, which means if we want to take the advantages of mode-locked fiber lasers, the super boarden or continous wavelength tuning in large scale, like 100 nm is necessary. A simple and easy to understand expliantion is:"create new frequency components to make the ultrashort output colorful". Accordingly, Nonlinear frequency conversion technique is the simpliest way to get continous wavelength in large scale to fulfill the needs of real applications like optical frequency comb.

There are three nonlinear frequency conversion methods:

1. Optical parametric oscillator (OPO)
2. GaAsnanowires based frequency conversion
3. Supercontinuum generation (SCG)

Optical parametric oscillator technique ultilize wave mixing features of the nonlinear crystals to achieve frequency conversion. OPO system pumped by mode-locking fiber laser has excellent properties in high repetition rate, high pulse energy, high conversion efficiency, large tunable scale and simple implementation. GaAs nanowires based frequency conversion technique is having semiconductor nanowires material interact with ultra short pulse. GaAs nanowires has special optical characteristic when it interact with ultrashort optical pulses, the nonlinear effect induced frequency conversion will extend the bandwidth multiplied. Supercontinuum generation is more ang more popular because of the super entend of the optical bandwidth and near-zero dispersion property in the micro-structrue fiber.

Chapter 3

Fundamentals of Dual-Comb Spectroscopy

In this chapter, we depict the time- and frequency-domain features of optical frequency comb firstly, the intrinsic connections of optical phase and carrier frequency are illustrated in detail. The demonstration provides the background we mentioned in Chapter 2 and natural connection between mode-locked lasers and optical frequency comb. The applications enabled by the property of optical frequency are discussed accordingly, the superiority of dual-comb spectroscopy is discussed in detail.

3.1 Concept, Properties and Applications of Optical Frequency Comb

We'd like to quote words from [44] that "Recently there has been a remarkable synergy between the technology of precision laser stabilization and mode-locked ultrafast lasers" to start the new chapter. The definition of optical frequency comb can be explained by imaging a frequency spectrum consists of a normal "comb" spaced by sharp frequency lines equally, and this frequency spectrum is produced by mode-locked lasers. Much work has been done to mode-locked laser and optical frequency comb [45–47], and ultimately led to the Nobel Prize in Physics which shared by John L. Hall and Theodor W. Hansch in 2005.

From Chapter 2 we know that the frequency spectrum of a mode-locked laser is a comb spaced equally frequency lines. However, to have a better understand optical frequency comb generated by a mode locked laser, one must setup the connection between the time- and frequency-domain [48]. Nonetheless, even before the demonstration, a key concept in the demonstration is carrier-envelope phase ϕ_{ce}. The absolute phase ϕ_{ce} is the phase

mismatch value between the peak of the envelope and the nearest peak of the carrier wave. If we regard an ultrashort pulse's time dependence electric field can be described as a fast oscillating sinusoidal signal, called the carrier, multiplied by a much more slowly varying envelope function in advance, which is written as $E(t) = \widehat{E}(t)e^{i\omega_c t}$. At the beginning, we assume the pulses are identical and the carrier-envelope phase is ignored. So for any pulse shape, the width of spectrum is inversely proportional to the width of temporal width of its slowly varying envelope. If one consider a train of identical pulses which are separated by a fixed interval, time of round trip, the spectrum of these pulses yields a comb of equally spaced frequencies, and the spacing is the repetition rate (f_{rep}) of the mode locked laser. We can easily see that the frequencies can be written as nf_{rep} where n is an integer. However in practice, ϕ_{ce} is evolving with time, Fig 3.1 depicts the envelope and the carrier of two subsequent pulses from a mode locked laser. The carrier wave propagates at constant phase velocity $\upsilon_p = c/n$ while the velocity of envelope is group velocity $\upsilon_g = c/n_g = c/(n + \omega\frac{dn}{d\omega})$ and repeats itself after the round trip time. Since $\upsilon_p \neq \upsilon_g$ in any dispersive medium, the time dependence electric field of pulse undergo a permanent increment, and this evolution between carrier and envelope can be explained by $dn/d\omega$ in group velocity. When the pulse train propagating through a piece of single mode fiber, L is the length of fiber with an index of refraction $n(z)$, the accumulated carrier-envelope offset is ϕ_{ce}

$$\Delta\phi_{ce} = [\frac{2\pi}{\lambda}\int_0^L n_g(z) - n(z)dz]mod2\pi = [\frac{\omega^2}{c}\int_0^L \frac{dn(z)}{d\omega}]mod2\pi \tag{3.1}$$

Here $\Delta\phi_{ce}$ is the so called carrier-envelope offset (CEO), representing the change of the absolute phase per round trip:

$$\Delta\phi_{ce}(t) = \phi_{ce}(t) - \phi_{ce}(t - T_R) \tag{3.2}$$

The concept of optical frequency comb in time- and frequency-domain is shown in Fig 3.1. One must not confuse the CEO phase $\Delta\phi_{ce}$ with the absolute phase ϕ_{ce}, which is defined under the consideration of a single pulse [49], i.e. such $\phi_{ce} = 0$ means that the peak of envelope and the carrier wave peak are at the same position for the certain pulse under the discussion. However, $\Delta\phi_{ce}$ is difference of the absolute phase ϕ_{ce} between two subsequent pulses, which can be also described as [50]

$$f_0 = \frac{\Delta\phi_{ce}}{2\pi} f_{rep} \tag{3.3}$$

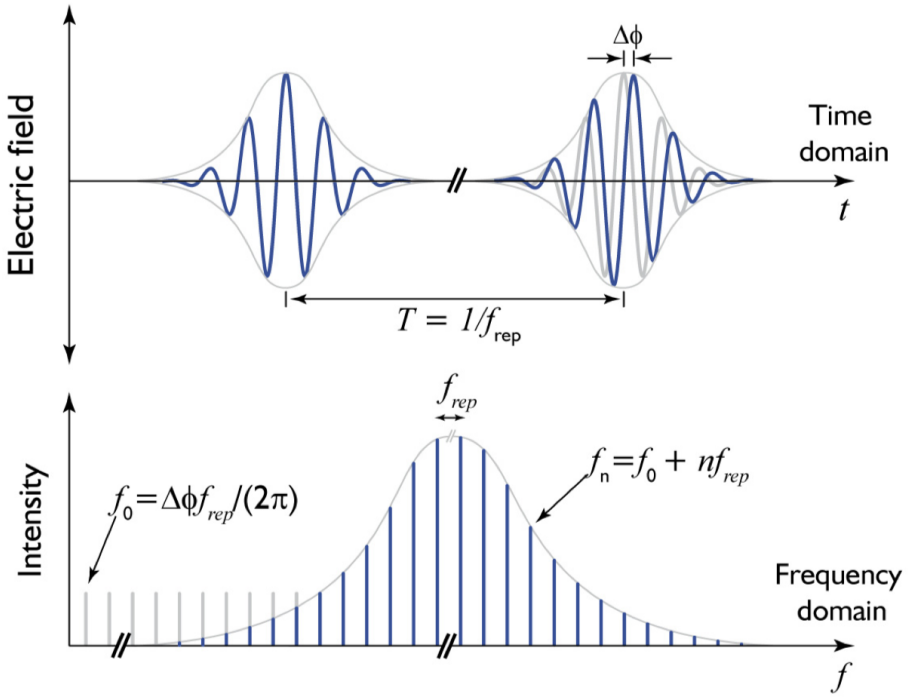

Fig. 3.1 Concept of optical frequency comb in time- and frequency- domain: a ultrashort pulses train generated from a mode-locked laser with the round trip time T. Δ_{ce} is clearly depicted between two subsequent pulses. The phase slippage of two absolute phase shift between the envelope and the electric field of the pulse leads to an carrier frequency offset $f_0 = \frac{\Delta_{ce}}{2\pi} f_{rep}$ [3]

.

where f_{rep} is the repetition rate of the mode-locked laser and equals the round-trip time T_R inversely. Therefore, the frequencies of optical frequency comb can be written as $nf_{rep} + f_0$, where n is an integer.

Until now, the fundamental of optical frequency comb has been demonstrated, and the two degree of freedom of optical frequency comb, f_0 and f_{rep}, are established. Any optical frequency comb will be revealed once the f_0 and f_{rep} are confirmed. Measurement method of f_{rep} is straightforward: the repetition rate detected by a fast photodiode while the most common approach for measurement of f_0 is heterodyne the fundamental and second harmonic. The method was first proposed by Telle et al [49]. The principle of this method is depicted in Fig 3.2. Taking the fundamental frequency comb line at the left side of the spectrum, $v_n = f_0 + nf_{rep}$, the second harmonic of this frequency comb line is $v_{2n} = f_0 + 2nf_{rep}$, the second harmonic frequency v_{2n} is beating with the $2 * v_n$, yields

$$2 * v_n - v_{2n} = 2 * (f_0 + nf_{rep}) - (f_0 + 2nf_{rep}) = f_0 \tag{3.4}$$

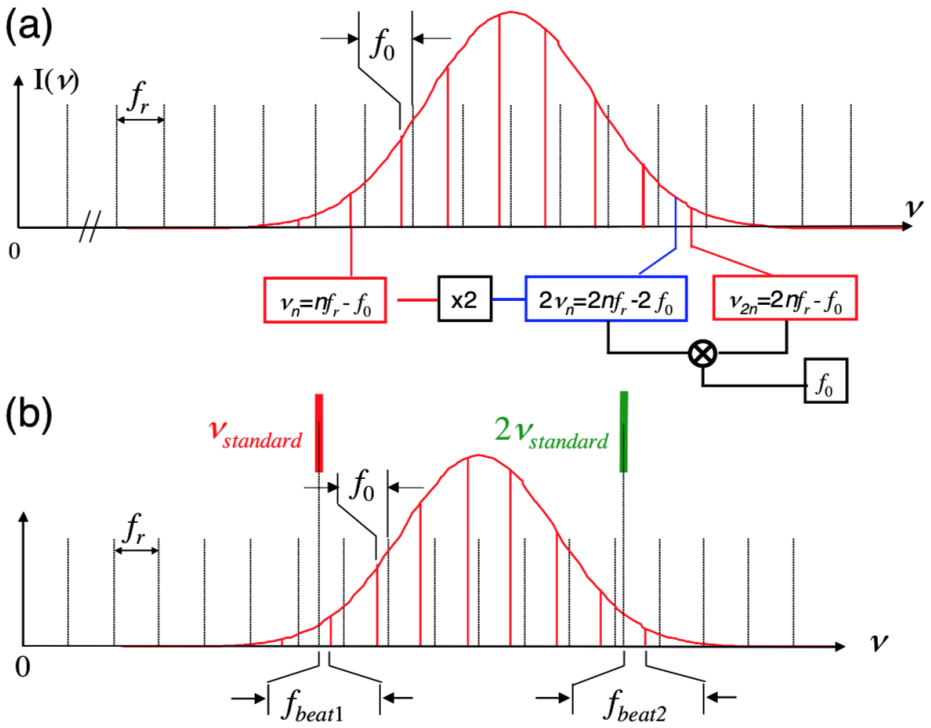

Fig. 3.2 Scheme for measuring the CEO-frequency of optical frequency comb generated by mode locked laser by heterodyning the fundamental and the second harmonic [4]

.

Equation 3.4 is the common method for measurement of carrier-envelope offset and are widely used [51, 52].

Optical frequency comb generated by mode locked laser has been proved as an excellent candidate for optical frequency metrology, frequency synthesis, clock-signal generation and precision spectroscopy. The long-term stable mode locked laser enables the significant simplification of an optical frequency comb, the most directly application for an optical frequency comb is optical frequency measurement. The high degree of precision and reliability support this new technology. Since the repetition rate of a mode locked laser has been proved that it strictly equals mode space within measurement uncertainty of 10^{-16} [45]. The uniformity of the comb line is robust even after experiencing strong spectral broadening in fiber, and the value has also been verified in [45]to a level below 10^{-17}. For absolute measurement of a single uncertain optical frequency, once the two degree of freedom, f_0 and f_{rep}, are established, then one can count the heterodyne beat between uncertain optical frequency and one of the comb lines. The explosion of absolute frequency measurement using optical frequency comb is not surprising, and we give a brief introduction on the most accurate devices based on optical frequency comb. First one is belongs to team of Max-

Planck Institute for Quantum Optics (MPQ) in Garching [53] in 2000, they took advantage of a transportable cesium foundation clock as OFC's reference. Other works include team from National Institute of Standards and Technology (NIST) in Boulder, Colorado can determine the frequency of an electric quadrupole transition of the Hg^+ ion less than 1×10^{-14} [54]. Similar accuracy on Yb^+ was reported by team at Physikalish-Technische Bundesanstalt (PTB) in Braunschweig [55].

3.2 Concept, Properties and Applications of Dual Comb Spectroscopy

One may consider that explore absolute frequency measurement system using optical frequency comb, indeed, optical frequency comb based on simple and energy efficient mode locked fiber lasers and super continuum generation can offer high accuracy and simple configuration frequency measurement for both academic and commercial use, which fulfill the goal of "high accuracy frequency measurements with low cost and easy implementation". We can establish a thulium doped soliton fiber laser induced super continuum generation to detect the absorption spectrum of carbon dioxide. The main method is based on Fourier transform spectroscopy. Fourier transform spectroscopy was proposed in the late 1950s while its basic spirit, the Michelson interferometry method was reported in 1887 [56].Up to now, Fourier transform spectroscopy is still the only technique in spectroscopy that keep the high resolution meanwhile provides broad spectra. The principle of the frequency comb based Fourier transform spectroscopy can be explained as follow: The output pulse trains generated from mode locked fiber laser is split into two equal part, then one of the beams is reflected by a mirror with fixed position while the second beam is reflected by another mirror on a movable platform. The interference signal can be detected by a photon detector. The spectral properties of the gas sample is contained into the interference signal which is usually called the interferogram. Now we analyze the advantages and drawbacks of the Fourier transform spectroscopy. One of its advantage is single acquisition with multitude of different measurements result from the broad spectral range offered by frequency comb. Besides, the frequency comb based Fourier transform spectroscopy possesses the short acquisition time, high detection sensitivity and high signal-to-noise ratio at the same time [5]. Here we depict the experiment principle and results from [5] in order to exhibit the supremacy of frequency comb based Fourier transform spectroscopy.

In fact, the performance of frequency based Fourier transform spectroscopy can be further promoted if one declines the acquisition time without affecting the other key parameters

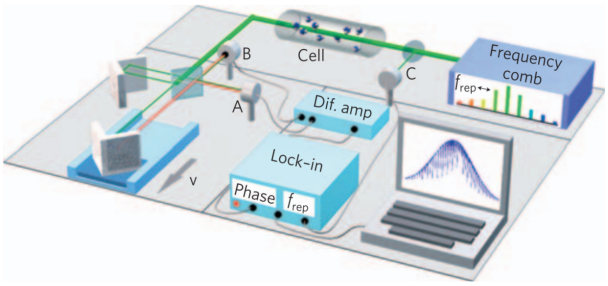

(a) Principle of the FC-FTS system.

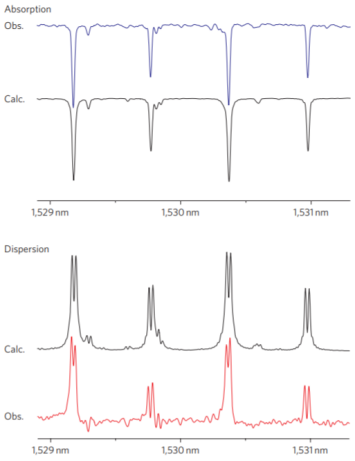

(b) Comparison between obseervation and simulation [5].

Fig. 3.3 Detector A and detector B measure the interference signal as a function of the difference between the optical path, and the frequency comb interacts with gas sample at first before spilits into two ways. All signals are synchronously detected at repetition rate with the output from detector C as reference. Comparison between obseervation and simulation, including absorpiton and dispersion plotted in a linear intensity scale [5].

like high resolution, compactness and broad spectral. There are some reports that using the combination of two slightly different frequency combs via electro-optical modulators with different modulation frequencies by Lee et al. in 2001 [57] or detuning the repetition rates distinctly by Schiller in 2002 [58] to realize the goal and the performance indeed get promoted. We start to introduce this new spectroscopy method, which is called multi-heterodyne spectroscopy commonly [59]. The direct combination of two frequency combs with an interferometric setup is a new method of Fourier transform spectroscopy, which provides the short acquisition time and high resolution spectroscopy at same time, meanwhile, circumvents the scanning implementation facilities by broad spectral bandwidth of frequency comb. The principle of this new method is "down converting tech" which as similar as traditional Fourier transform spectroscopy. Generally, one or two frequency combs interact with gas sample then overlapped with each other. The interference signal yields a comb in the radio frequency domain and the signal can be detected by a simple photon detector. Afterwards, the output signal of photon detector is called interferogram contains the absorption information of the gas sample under study, the information is revealed by applying Fourier transform algorithm. Assuming that two frequency combs have slightly different repetition rates $f_{rep,1}$and $f_{rep,2}$ and $f_{rep,1} - f_{rep,2} = \delta$ for the sake of simplicity, where δ is the separation of two repetition rates. The interference signal detected by photon detector generated by beating happened

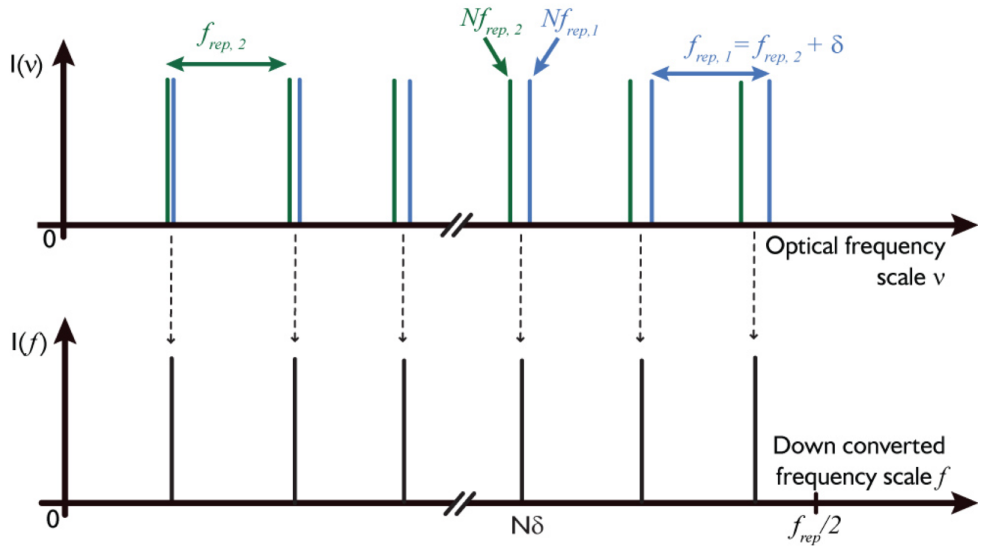

Fig. 3.4 Downconversion of the optical frequencies. Two frequency combs with slightly different repetition rates $f_{rep,1}$ and $f_{rep,2}$ are superimposed and form a beating comb in the radio frequency domain. Hence, the optical frequencies are down-converted to radio frequencies by the scaling factor that is dependent of the detuning of the combs' repetition rates [6].

between all optical modes in both frequency combs. If only the beating between the comb line with the same order n are considered, the absolute frequency of the beating can be written as

$$f_{n,1} - f_{n,2} = (f_{0,1} + nf_{rep,1}) - (f_{0,2} + 2nf_{rep,2}) = f_{0,1} - f_{0,2} + n\delta \tag{3.5}$$

Therefore, the optical frequencies is down converted into radio frequency domain so that they can be easily detected by a photon detector. The principle in time- and frequency-domain are depicted in Fig. 3.4 and Fig. 3.5. In fact, every comb line beats with other comb lines and create a new frequency component in radio frequency domain when two optical frequency combs are superimposed and interact with each other, which means the beating is not only generated by $f_{n,1}$ and $f_{n,2}$, but between $f_{n,1}$ and $f_{n-1,2}$, $f_{n,1}$ and $f_{n-2,2}$ or $f_{n,1}$ and $f_{n+1,2}$ as well. Therefore we need choose suitable value of the down converted radio frequency by control the frequency position of the comb lines. Assuming that only first frequency comb passes through the gas sample and experiences phase shift and intensity attenuation, afterwards, the first frequency comb is overlapped with the second frequency comb. Meanwhile, we use the format we mentioned before in this section that the time dependence electric field of a frequency comb. Therefore, the two electric fields of these two combs sum up to:

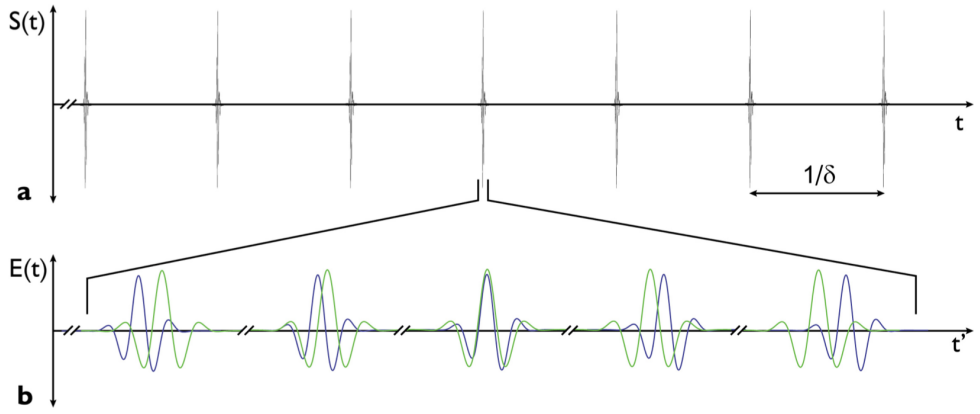

Fig. 3.5 Dual comb spectroscopy in time domain and the formation of interferogram: Because the two lasers have different repetition rates, the pulses of the two lasers are slowly sliding over each other (b). Here, the interaction of the first laser with the gas sample is indicated by a phase shift and attenuation of the corresponding pulse train (blue) in respect to the pulse train of the second laser (green). The bursts are generated when two pulses of each frequency comb, respectively, arrive at the detector at the same time (a). Between these incidents, there is almost no signal for a long time until the next two pulses arrive and form a burst. The period of the bursts is inversely propotional to the separation of repetition rates, $\frac{1}{\delta}$ [6].

$$E_1(t) + E_2(t) = \sum_n [A_{n,1} e^{-\alpha_{n,1} - i\phi_{n,1}} e^{-(2\pi f_{n,1})t} + A_{n,2} e^{-(2\pi f_{n,2})t}] \tag{3.6}$$

By using a low-pass filter, one can make sure that only the beating generated by the same order n^{th} comb lines and form the interferogram after the photon detector [6].

Generally, a relatively long acquisition time, a narrow comb bandwidth, and a high repetition frequency leads to a positive impact on resolution for dual frequency comb based Fourier transform spectroscopy. It is worth to note that the gas sample under study is probed at discrete optical frequencies corresponding to the lines of the frequency comb in frequency domain, which also means that the molecular spectrum is sampled spacely at the repetition rate of the frequency in time domain. To make sure that the observed molecular lines is not concealed within the comb lines if the linewidth of the molecular transition is too small, the requirement for the repetition frequency has to be chosen less than the half width of the molecular transition at half maximum in order to sample the molecular transitions properly.

In summary, this chapter introduces the background and principle of optical frequency comb (OFC), Fourier transform spectroscopy (FTS), frequency comb based Fourier transform spectroscopy (FC-FTS) and novel method – dual comb spectroscopy (DCS), respectively. The advantage of DCS including short measurement time, high sensitive and simple configuration

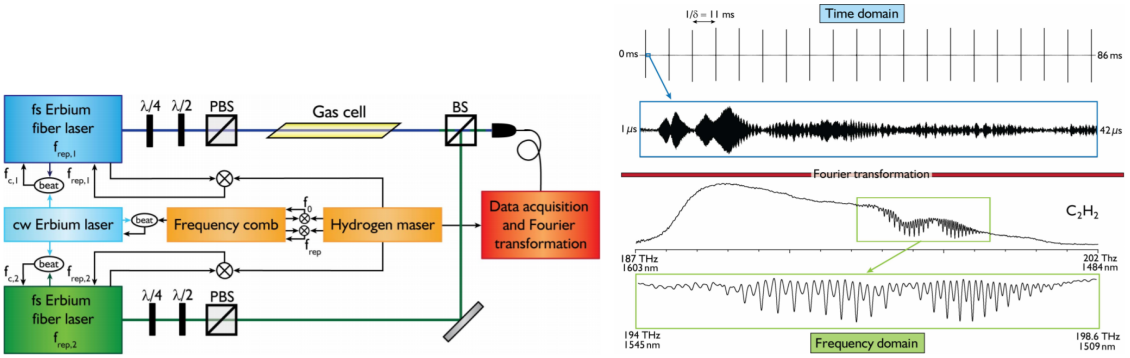

(a) Complete experiment setup of DCS system based on Erbium fiber laser.

(b) Interferogram and result spectrum of a single shot measurement

Fig. 3.6 Demonstration of DCS system in practice [6].

are demonstrated, and the supremacy of mode locked laser as a seed source for frequency comb is discussed as well, which naturally leads to the next chapter on the experiment mode locked fiber laser and DCS based on that.

Chapter 4

Bi-directional Soliton Fiber Lasers

This chapter we will focus on the bi-directional mode-locked fiber lasers, the fundamentals and previous work done by others are introduced at first, then we have discussion on the first bi-directional mode-locked fiber laser in2 μm, including configuration, CNT saturable absorber, result analysis. The unique property that two counter circulating pulse trains have slight repetition rates, which enables bi-directional mode-locked fiber laser as an excellent candidate, is demonstrated, the possible causes such as unbalanced configuration, fiber birefringence, group delay dispersion are discussed.

4.1 Pervious work on Bi-directional Soliton Fiber Lasers

Ultrafast fiber lasers generating ultrashort optical pulses have been studied for several decades because of the special features including compact design, extraordinary robustness and low cost, which have enabled a wide range of applications such as material processing, precision metrology and medical imaging. Passive mode-locking technology (see section 2.2)is one of the most common methods that we used to generate the ultrashort pulses via different saturable absorbers (SA). There are different kinds of SAs commonly used in fiber lasers in order to generate ultra-short pulses and we'd like to remind again including semiconductor saturable absorber mirrors (SESAM) [20],carbon nanotube/graphene [21–23], Molybdenum disulfide (MoS_2) [24], in addition to these natural material-based SAs, there are some artificial methods be widely used as well, such as nonlinear optical loop mirrors [NOLM] [18] and nonlinear amplifying loop mirrors [NALM] [19], and most used one, nonlinear polarization rotation [60].

Since most of the ultrafast lasers generate pulses in a single direction, by inserting an optical isolator into the cavity to guarantee the unidirectional operation via back-reflection suppression. Besides, using an optical isolator will decrease the self-starting threshold as well

which could enhance the mode-locking regime [25]. the novel approaches and observations of bi-directional ultrafast lasers have also gained great interest for sensing applications, such as optical fiber gyroscope for rotation measurement [61] and dual-comb spectroscopy (DCS) for precise gas detection [3]. DCS requires two phase locked optical frequency comb with slightly different repetition rates interfere with each other, which could offer excellent gas absorption spectroscopy result in radio frequency domain using simple analyze method "down converting" technology [62]. The implementation require two optical frequency comb with high coherence and phase locked, and the bi-directional mode locked fiber laser could satisfied this basic requirement with simple configuration.

Conventionally, the implementation of optical isolator inside the ring cavity of mode-locked fiber laser guarantees the unidirectional propagation. However, to bridge over sensing applications and mode-locked lasers, the bi-directional mode-locked fiber lasers are also attractive. It was in 1967 that the first bi-directional mode-locked laser was invented by Buholz and Chodorow as a gyroscope-based sensor [63]. As for all-fibred bi-directional mode-locked ring fiber laser, Kieu and Mansuripur presented at first time in 2008 [10]. In this paper, a short segment of a 22 mm long fiber taper embedded in carbon nanotubes/polymer composite as a saturable absorber [64], the inspiring observations such as the average power difference, the repetition rates separation, and the beating note from two outputs are demonstrated and the "share cavity" is certified as sensing application devices. This paper confirmed the effective of bi-directional mode-locked fiber ring laser even though the unstable optical spectrum was not solved at that time. After that, Braga et al. demonstrated a novel method to control the crossing points of the two independent counter circulating pulses actively [7], mode locking is achieved by using two amplitude modulators driven by a signal regenerated from the laser oscillation. The active feedback implementation enables the stabilization for pulse crossing points, and the elimination of bias beat note, the relationship between beat node and voltage applied to the modulator is demonstrated as well. More recently, various bi-directional mode-locked fiber ring lasers are reported. C. Ouyang et al. present an all-fiber bidirectional mode-locked soliton fiber laser with independent saturable absorber for each propagation direction [9]. Mode locking is achieved by incorporating two different semiconductor saturable absorber mirrors (SESAMs) as well as a polarization-independent four-port circulator. The discussion on intracavity loss control reveals the unbalance cavity configuration has a significant impact on performance of bi-directional mode locking. Soon after that, Venkatesh Mamidala et al. [65] achieved bi-directional operation using graphene-based saturable absorber with a similar configuration with [9]. The different propagate experience leaded by asymmetry for both direction can be adjusted independently by change the parameter between port of circulator and saturable absorber.

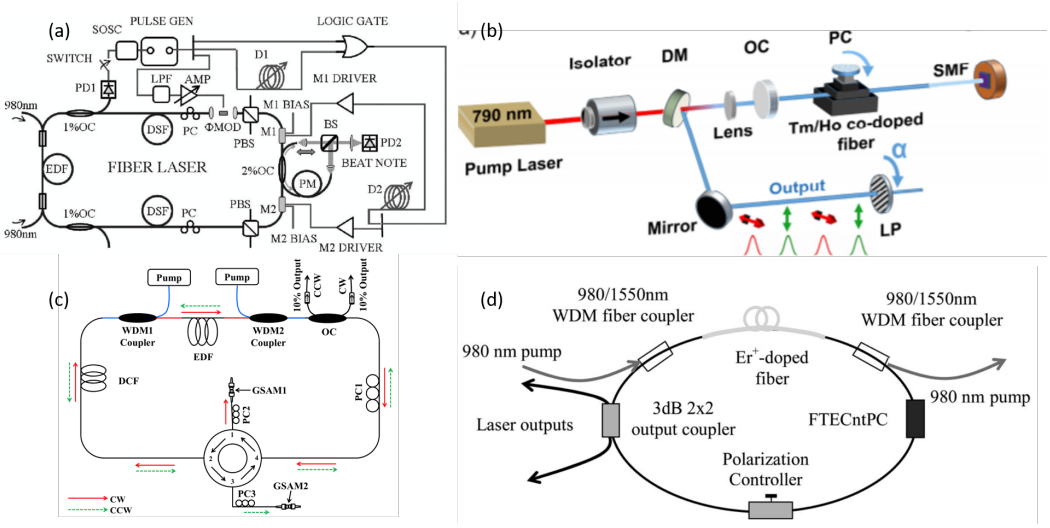

Fig. 4.1 Previous works on bi-directional mode locked fiber lasers. (a): image from [7] ;(b): image from [8]; (c): image from [9]; (d): image from [10].

These two paper mentioned above are excellent sample for study of bi-directional mode-locked fiber ring laser, but the intrinsic mechanism which lead to variation in optical spectra, pulse duration, average optical power and especially, the repetition rates are covered since the variables in sub-path are controlled according to direction. Refocusing on the isolation-free configuration again, Zeng et al. [66]chose carbon nanotube as saturable absorber meanwhile using similar configuration with Kieu. In this paper, the output spectrum have at most 10 nm separation for opposite direction, and the lasing regime can transfer from C band to L band by only tuning polarization controller in the cavity. Besides, the repetition rate difference in opposite direction can be controlled in the range of 10 Hz to 50 kHz. This paper studied the birefringence's role in bi-directional mode locked fiber ring laser, but the details has not been revealed yet. Almost all works mentioned above suffer from the temporal/spectrum output fluctuation and long-term running disability. Several works have been reported for stable temporal/spectrum output and investigation on the differentiation in counter circulating direction. Maria Chernysheva et al. [67] presented a novel switchable uni- and bi-directional hybrid mode-locked fiber ring laser with single-wall carbon nanotubes and nonlinear polarization rotation. It is worth mentioning that NPR method in this paper is realized by polarizing optical fiber and two polarization controllers. By using precise control of the state of polarization (SOP) in the cavity enable the losses variation for opposite soliton. The author indicated the configuration guarantees the soliton pulses quality and the operation stability. A. A. Krylov et al. [68] demonstrated the gyroscopic effect in a bidirectional erbium-doped all-fiber soliton mode-locked laser, with high rotation sensitivity.

Although robustness opposite pluses generation of bi-directional mode locked fiber lasers have been successfully demonstrated by different groups in the past ten years, including the experiments and observations in 2 μm is rare, until now there is only one published report on thulium-holmium fiber laser based dual comb generation [8], which using two orthogonally polarized interlaced pulses train to generate the coherent rf comb. Compared with 1.55 μm, 2 μm wavelength region has unique properties water absorption and retina-damage prevention that enable it cover, but not limited to free space optical communications, laser imaging for detection and ranging (LiDAR), surgery and precise gas detection such as water and carbon dioxide. Here by, we demonstrate a bi-directional ultrafast thulium-doped fiber laser, generating picosecond pulses (1ps) in both clock-wise (CW) and counter clock-wise (CCW), the laser is passively mode locked by using carbon nanotube polymer film. The mode locking for both direction can be achieved simultaneous with enough pump power and fine polarization status tuning. The result indicates that the potential application of 2 μm mode locked fiber laser in bi-directional running mode such as precise rotation sensing and dual-comb spectroscopy.

4.2 Scheme on 2um Bi-directional Soliton Fiber Laser

The bidirectional thulium-doped mode-locked fiber laser setup, as shown in Fig. 4.2, a 2.5-meter-long piece of thulium-doped silica fiber (TDF) (OFS, TmDF200) is used as the gain medium with an estimated anomalous dispersion of $-0.02 ps^2/m$ at 1960 nm region. The TDF is pumped through a wavelength-division multiplexing (WDM) coupler (OPNETI 1570/2000nm) using unidirectional pumping with the pump light going in the clockwise (CW) uni-direction. The pump source is an external-cavity tunable laser (Photonetics, TunicsPlus) operating at 1570 nm and amplified by a high-power Erbium-doped optical fiber amplifier (Keopsys, KPS-BT2-C-37). To realize ultrashort pulses generation, a thin film CNT based saturable absorber was inserted into the cavity vertically. The arc-discharged single-walled carbon nanotubes were dispersed by using Carboxymethyl cellulose (CMC) as a surfactant [69]. The resulting CNT polymer film hosted by CMC has a strong absorption around 1960 nm. Figure 4.3 shows a good absorption property in 2um region. Two fiber optical patch cord (Alnair-Labs, FC/APC-FC/APC) with angled fiber connectors are used to sandwich the CNT thin film, while two connectors were mounted on FC/APC to FC/APC L-Bracket (Thorlabs, ADAFCB3), the FC/APC-CNT-FC/APC sandwich structure with fixed on an independent optical breadboard which is good for environmental stabilization. A 2*2, 50/50 coupler is used to split the pulses from the ring cavity in each direction. There is no optical isolator (ISO) is used in the cavity so that the laser could delivering

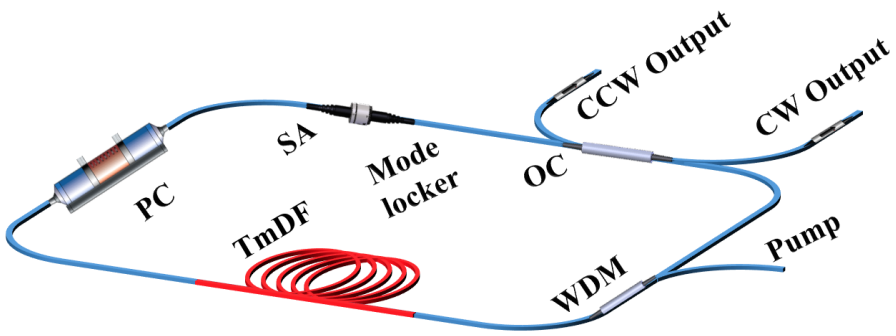

Fig. 4.2 Scheme of bi-directional soliton fiber laser. WDM: wavelength division multiplexing; TmDF: Thulium doped fiber; PC: polarization controller; SA: saturable absorber; OC: output coupler

both directional pulse trains in the cavity, clockwise (CW) and counterclockwise (CCW), respectively. However, the optical isolators are added at the outputs in bidirectional to prevent unwanted reflections into the cavity. A three paddles type polarization controller (PC) is employed to optimize the mode locking conditions by change the polarization status in the cavity. The pigtails of all the passive fiber components are made of single-mode fiber (SMF) (Corning, SMF-28) with an estimated anomalous dispersion of $-0.06ps^2/m$ at 1960 nm. The total group velocity dispersion of the cavity is in the negative regime, which enables the soliton pulse generation. An optical spectrum analyzer (YOKOGAWA AQ6375) and digital oscilloscope were connected to the output port. The mode locking status in both direction could be achieved simultaneously when the pump power is raised above the threshold by adjusting the polarization controller very carefully.

It is also worth to note that when the polarization is fixed, the counter-circulating pulses preferred to cross each other at the postion of saturable absorber. The mechanism of this intrinsic behavior can be explained as follow. Mutual saturation of the absorber for both directions leads to a lower loss experienced by the pulses, which is so-called collding mode-locking mechanism.

Figure 4.4 shows the outputs spectra of the laser measured by optical spectrum analyzer with an optical resolution bandwidth of 0.05 nm. Since the dispersion of the laser is anomalous, both directional spectrum has the typical soliton spectrum with Kelly sidebands can be observed when the pump power is set to 109 mW. The central wavelength of the opposite direction is a little bit different, for CW direction, the central wavelength of the soliton pulse is 1958.62nm, while the central wavelength of the soliton pulse for CCW direction is 1962.34 nm and the opposite directions have a central wavelength gap of 4 nm. The soliton spectrum for both direction has a 3 dB bandwidth of 4 nm. The result of different type output indicates the different propagation experience and the cavity asymmetry, which

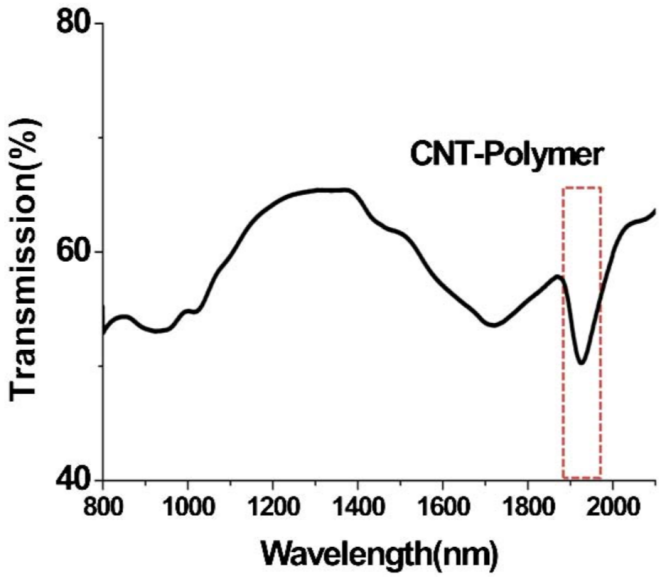

Fig. 4.3 Transmission spectrum of the CNT-incorporated CMC thin film [11].

will be explained in details later. We also measured the repetition frequencies using an RF spectrum analyzer (Agilent, E4440A). Figure 4.2 shows that the RF spectra of bi-directional outputs, the repetition rates of the CW direction and the CCW direction are 25.0185 MHz and 25.0610 MHz, with the difference around 40 kHz as shown in Fig. 4.5. The difference of two repetition rates, Δf_{rep} could be changed by tuning the polarization controller and has the range from 10 Hz to 50 kHz. The difference of the opposite direction RF spectrum result is mainly contributed the group delay dispersion theoretically, since the we have the info about group velocity dispersion (GVD) on thulium doped fiber and SMF-28, which is $-0.02ps^2/m$ and $-0.06ps^2/m$, the cavity dispersion calculation result (-195 ps/(nm km)) indicates that for each nanometer wavelength change of opposite direction, with one kilometer propagation distance, the group delay of two pulses should be 195 picosecond. With the information of cavity length and central wavelength separation, one can easily get that the repetition rates separation induced by group delay should be around 3 kHz, the calculation detail is as follow

$$\Delta f = \Delta\lambda |D_{total}| (2\pi c f^2/\lambda_0^2) \tag{4.1}$$

where D_{total} is the total dispersion of the segmants of the fiber that the different pulses pass thorough, here should be the total dispersion of the cavity.

Therefore, the theoretical calculation 3 kHz has a big difference with the result recorded by the analyzer, which is around 40 kHz. There must be other factors contribute to the bias on repetition rate.

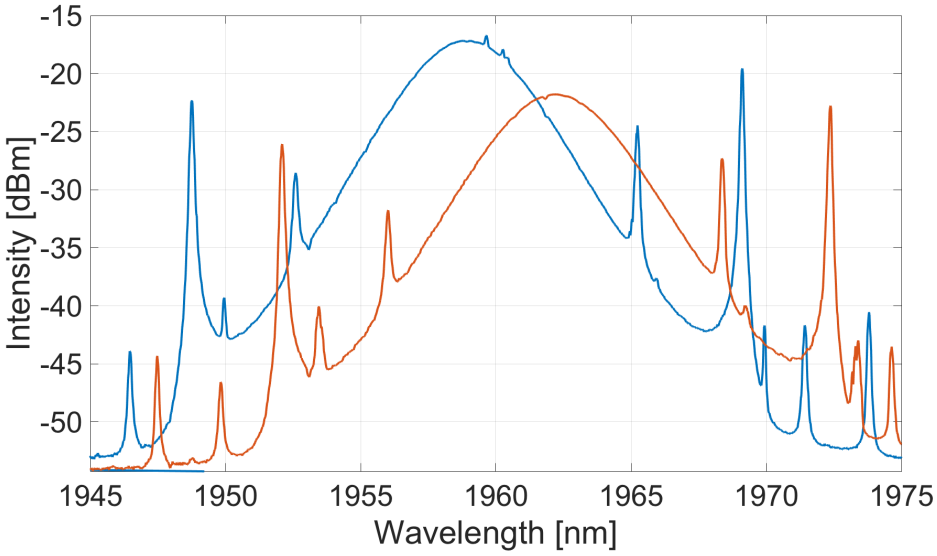

Fig. 4.4 Optical spectrum of CW and CCW direction

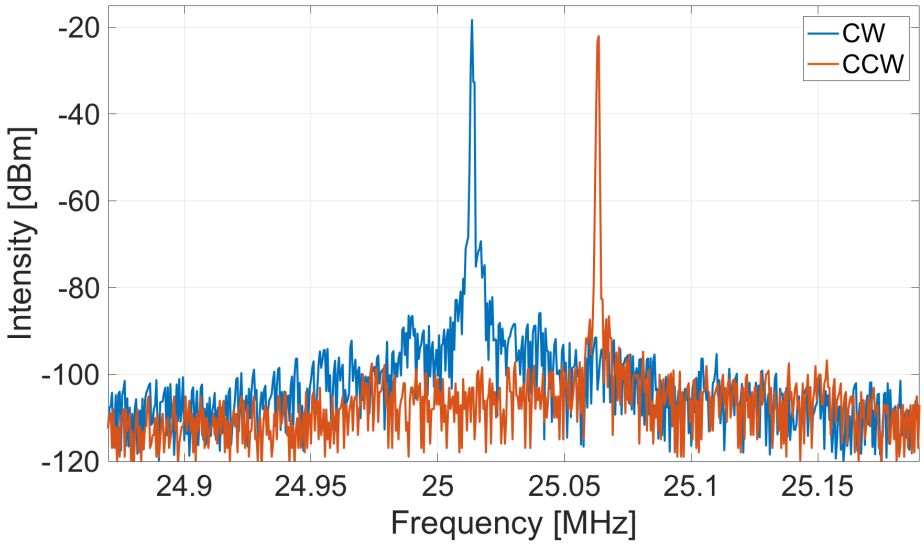

Fig. 4.5 Repetition rates of CW and CCW direction pulse trains

4.3 Central Wavelength Different and Separation in Repetition Rates

We can start from the unbalanced configuration. In general, the CW pulses are amplified by thulium doped fiber at first, before passing through the 50/50 two by two output coupler, and passing through CNT eventually, while the CCW pulses will pass through all components reversely. Consequently, two opposite pulse would always have the different peak power when reaching the CNT saturable absorber, which will lead to potential non-saturable absorption in different level [68]. Different from configuration in [9] which achieved the bi-directional mode locking operation mode by using a four-port circulator instead of sharing the single cavity, although the bi-directional mode locking operation mode is not in the single cavity, the analyze and explanation for different features is also work for our laser setup. It is worth to note that during the setup and splicing period of the ring cavity, the different conjunctive sequence of components will lead to totally different results. For instance, the different positon of CNT based mode locker in the cavity would contribute to the different operation mode based on the experiment record: when we put mode locker after gain fiber and output coupler (from CW direction), in other words, when the output coupler is sandwiched in between gain fiber and mode locker, the favored and suppressed direction achieved by fine tuning the polarization controller, which reveals the similar result with [67] that the bi-directional operation could only available for continues wave regime while only quasi-unidirectional operation have been generated in conservative soliton regime as shown in Fig. 4.6, the dominating one direction over another is unchangeable because of the cavity asymmetry; However, when we using the schematics like figure 4.2, the mode locker was inserted between PC and output coupler, the bi-directional operation could be achieved in soliton regime, and the power ratio is 15dB, the result is similar with [70].

Therefore, the unbalanced cavity design makes contribution to the 40 kHz separation. So there is another aspect of explanation for the bi-diretional soliton mode-locked fiber ring laser, if we consider the intensity variation of counter-propogating soliton leads to the difference refractive index, according to Kerr-effect in the silica fiber. Actually, there is another operation mode exists during the experiment, the laser tends to operate in a CW direction as depicted in Fig. 4.6. Only CW direction generates soliton with the average optical power over 1 mW, whereas the average optical power of the opposite direction is only hundreds of microWatts. The optical spectrum of CW and CCW directions center at 1950 nm and 1952 nm, respectively. With the similar bandwidth at the 3-dB level of 4.3 nm and 6 nm, correspondingly. Besides, identical position of Kelly side-bands, proving soliton generated in both directions while CW is highly dominated direction. Under this circumstance, the

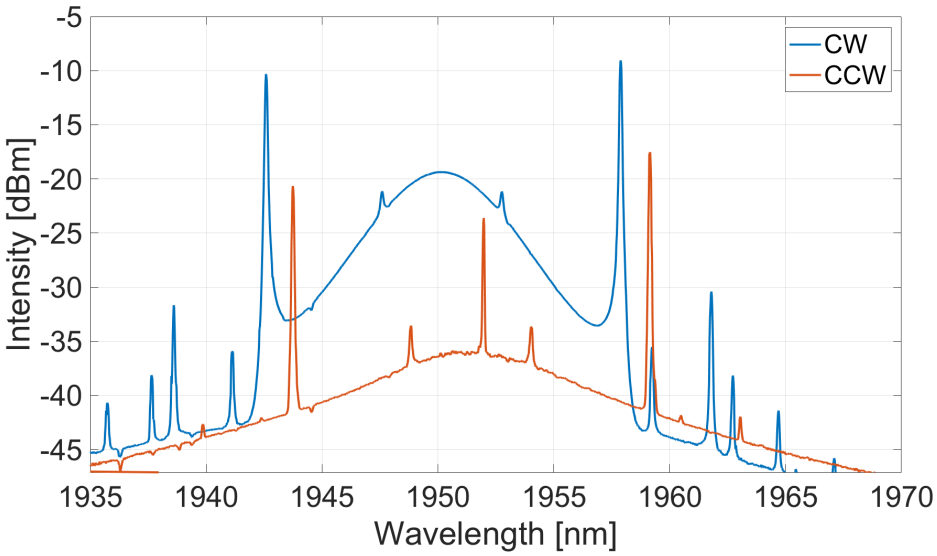

Fig. 4.6 Mode-locked output at dominating CW direction mode

SNR from rf spectrum and the amplitude from oscilloscope is significant small for CCW direction and the autocorrelation trace is disabled since the low output power of CW direction. This unidirectional dominating phenomenon was also observed and reported in [67]. Due to significant power difference between the CW and CCW directions, the nonlinear part of refractive index for the counter-propagating pulses is different. Ideally, the repetition rate of regularly spaced train of pulses in mode-locked laser with a ring configuration can be written as: $f_{rep} = c/(nL)$. The nonlinear optical Kerr-effect indicates that the refractive index n in active medium consists of linear n_0 and second-order nonlinear refractive index n_2 where $n = n_0 + n_2 I$, where n_2 has a order of $10^{-16} cm^2/W$ for silica fibers at 2000 nm wavelength range. Therefore, the different intensity leads to different fundamental frequencies eventually.

In a short summary, the repetition rates of opposite direction should be different, factors may including group delay dispersion since the central wavelength is different, unbalanced configuration, Kerr-effect in the silica fiber, fiber birefringence and polarization dependent dispersion. In the previous works which have the similar configuration with our setup [68] and [70] the results all revealed that the reverse propagation experience and different contribution of intracavity GVD [70, 71].

Except for unidirectional operation mode, bi-directional mode can still be achieved by adjusting the polarization controller. We achieved another stable operation mode that CW and CCW direction have almost the same center wavelength and repetition rate. The state of polarization under this circumstance is fixed in order to create the enough fiber birefringence to balance the intensity variation induced refractive index change or group delay dispersion

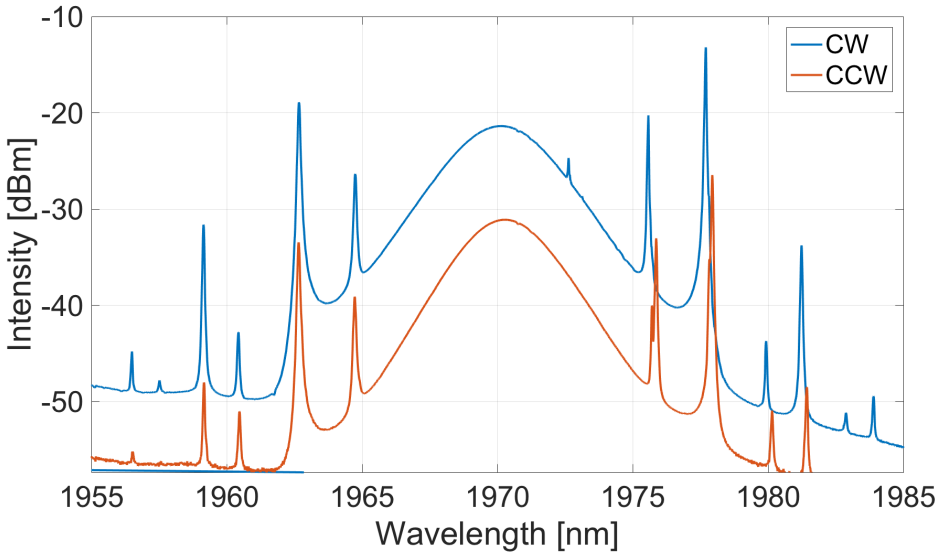

Fig. 4.7 Optical spectrum of CW and CCW direction with slightly difference on center wavelength

Table 4.1 Comparison in f_{rep} separation and λ_0 among different experiments.

$\Delta\lambda_0$	f_{rep} separation result	Beating signal
Superimposed [10]	0 Hz	2 MHz
$>$ than 15 nm (situation 1) [66]	791 Hz	Not mentioned
2.8 nm (situation 2) [66]	137 Hz	Not mentioned
Superimposed (situation 1) [68]	0 Hz	67 kHz
Superimposed (situation 2) [68]	0 Hz	400 kHz
Superimposed [70]	0 Hz	280 kHz
Superimposed [72]	0 Hz	400 kHz

induced repetition rate separation. Since the output power of CW and CCW direction are still different, the value of average optical power of CW and CCW direction is 4.5 mW and 0.9 mW, respectively. The central wavelength of the opposite direction is a little bit different, for CW direction, the central wavelength of the soliton pulse is 1970.28nm, while the central wavelength of the soliton pulse for CCW direction is 1970.14nm under 133.5mW pump power, opposite directions have a central wavelength gap of 0.14nm. The soliton spectrum for both direction has a 3dB bandwidth of 3.5nm. However, the similar optical spectrum for both directions is depicted in Fig. 4.7 and the similar repetition rate result is depicted in Fig. 4.8. The relationship between central wavelength difference and repetition rates separation in equation 4.1. The calculation is 10.75 Hz, which has a pretty good match with the data from Fig. 4.8.

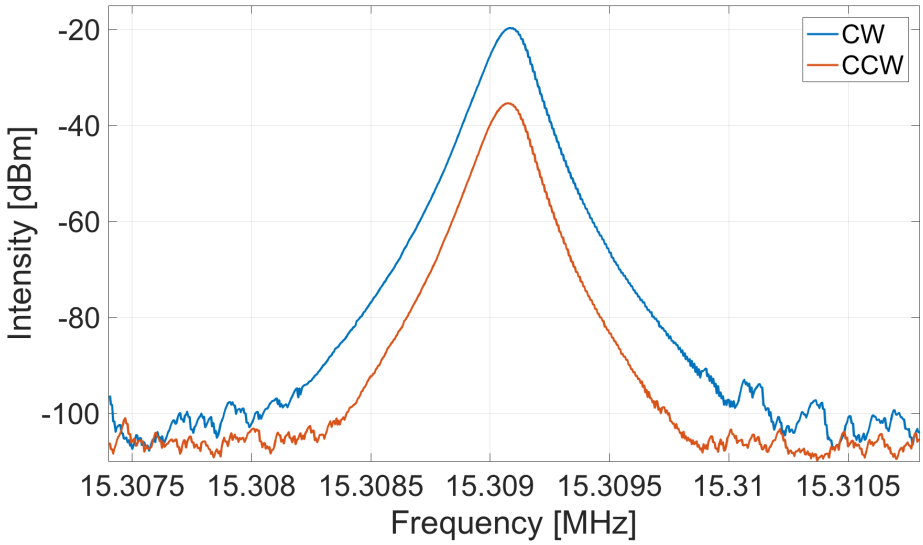

Fig. 4.8 Repetition rates of CW and CCW direction pulse trains with slightly difference

Table 4.1 indicates that the beating note of CW direction and CCW direction mainly caused by the uncertain and unstable carrier phase relationship between two pulse trains. The efforts on controlling the beating signal reveal the fact that it is not easy to lock Δf_{CEO} between CW and CCW direction and get the suitable f_{rep} separation at the same time by introduce the group delay dispersion and other effects.

It is also worth to note that the absence of an optical isolator in the cavity and environment sensitivity of single mode fiber, our bi-directional mode-locked laser system is extremely sensitive to the arbitrary perturbations, and this sensitive highly affect the stability of the laser. In fact, almost all the experiment have been reported have the stabilization issues more or less. A lot of factors affect the stabilization of bi-directional mode-locked fiber laser including the strong feedback and saturable absorber is too thick, which is corresponding to the colliding pulse mechanism we mentioned before. It is a pity that we can not get stable output pulse trains to generate the beat signal, or try to test the carbon dioxide assorption property in 2000 nm wavelength region so far, but we will keep working on that in the future.

In summary, this chapter bring forward the advantage of bi-directional soliton fiber laser in setup the dual-comb spectroscopy and review the previous works done by other researchers. Afterwards, the isolator-free soliton ring Tm fiber laser with simple configuration is purposed, the result and factors that contributes to slightly different repetition rates in two direction are analyzed and the beating signal explanation is demonstrated as well.

Chapter 5

Self Laser Line Sweeping in Tm Fiber Ring Laser

The spontaneous laser line sweeping (SLLS) phenomenon is demonstrated in this chapter. The SLLS phenomenon and the previous work on that are introduced at first. Spatial hole burning (SHB) effect and parasitic relaxation oscillation are discussed under the simple ring isolation-free laser cavity. The influences of pump level, polarization state are depicted accordingly.

5.1 Spontaneous Laser Line Sweeping in Fiber Laser

In a fiber laser whose configuration ensures existance of standing waves for single or multiple longitudinal mode(s), The population inversion is less depleted at nodes where the intensity is always minimal than the anti nodes where the intensity is maximum. Assume that currently the longitudinal mode v_i is the selected mode oscillating in the cavity, the formation of standing wave at mode v_i will result in the depletion of population inversion at antinodes. Therefore, the initiate mode v_i is less preferred because the decline of gain, which is called spatial hole burning (SHB). In case of wide spectral band gain like doped fiber lasers, the decline of gain in active mode v_i will lead to rise of adjacent longitudinal mode v_{i+1} or v_{i-1}. The hop of longitudinal mode leads to the evolvement of output laser wavelength.

Self wavelength sweeping or spontaneous laser line sweeping (SLLS) is one of intrinsic instabilities occurs in fiber laser, which have been reported in 2011 by for the first time. SLLS effect was observed in ytterbium fiber lasers at first [73, 74], the similar experiment results in erbium [75], thulium-holmium [76], holmium [77] and bismuth fiber lasers [78]. The FabryPerot cavity configuration, using perpendicularly cleaved fiber ends [75], one

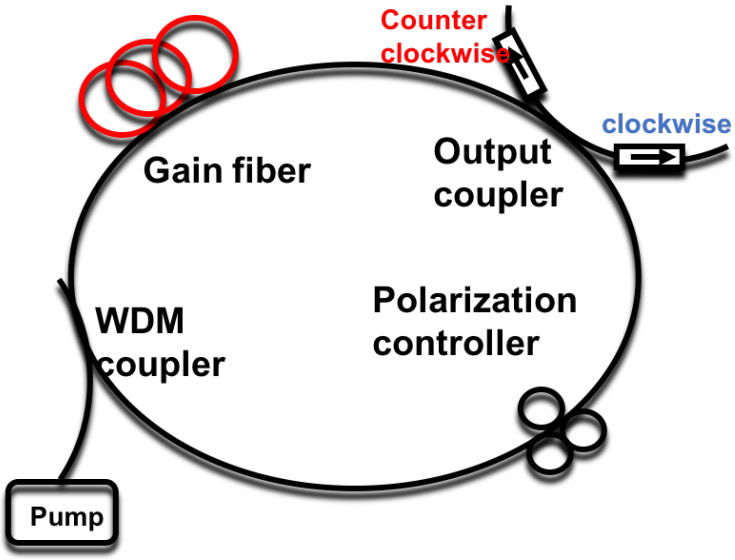

Fig. 5.1 Configuration of self sweeping laser

high-reflectivity mirror, narrowband fiber Bragg grating (FBG) [73] or fiber loop mirror (FLM) formed by a optical coupler [73, 76, 79] has been widely used in SLLS fiber laser. Record on fiber laser with ring configuration is rare since we usually insert an optical isolator inside the ring cavity to prevent the unwant refleaction which conflict with the mechanism of SLLS effect in fiber laser. Generally, SLLS in fiber lasers can be ascribed to spatial-hole burning (SHB) in the active medium when countercirculating, narrow-linewidth light waves are superimposed, it results in the creation of standing-wave in the cavity. The antinodes and nodes created by standing-wave experience different saturation in the gain medium, the gain is saturated easily in the antinodes so that iniaiate longitudinal mode is less preferred compared with its adjacent longitudinal modes.

5.2 SLLS in Tm Fiber Ring Laser

Our mode-locked fiber laser is just worked in a counter-circulating way. At first, when we built up the contiouns-wave fiber laser before inserting the carboon nanotube to initiate the mode locking, the configuration is shown in Fig. 5.1. Superisingly, the outputs from optical spectra analyzer (YOKOGAWA AQ6375) have a strong wavelength self-sweeping trend instead of quasi-stable narrow linewidth state as shown in Fig. 5.2.The sweeping range can be controlled by the pump power from 10 nm to 15 nm, whereas the sweeping rate is relatively slow compared with other experiment results, the period of single sweeping is in the range of 220 s to 240 s depends on the pump level and the polarization state inside

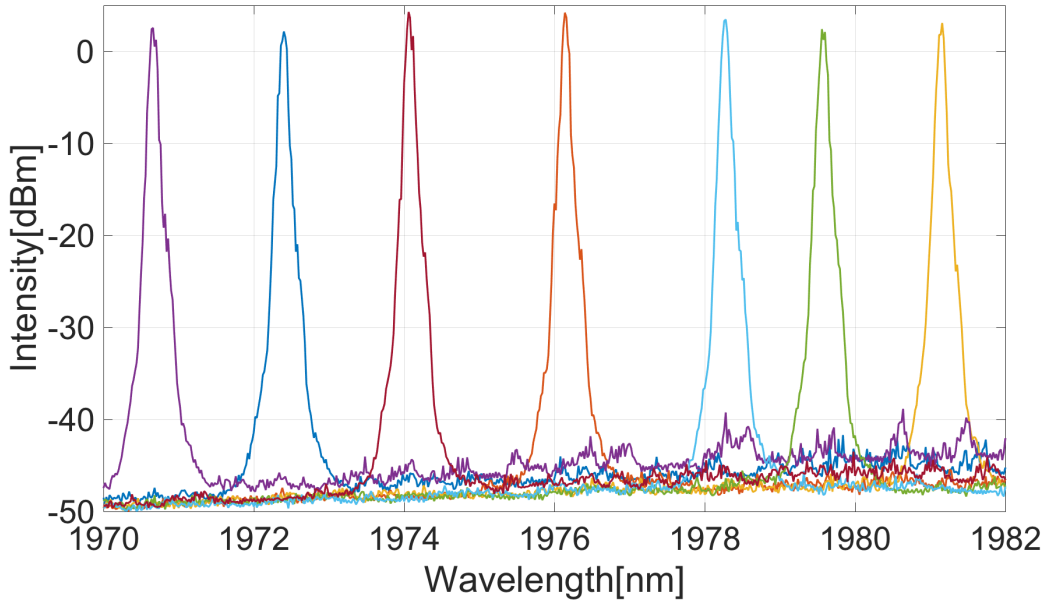

Fig. 5.2 Wavelength evolvement in one sweeping period

the cavity. The sweeping rate is significant accelerated to 70 s 100 s when we replace the 2*2 50/50 output coupler by a 2*2 80/20 one while the pump power is the same. Each laser narrowline has bandwidth with 0.06 nm, the sweeping direction is from long wavelength to short wavelength The observation results indicate that the self-sweeping related to the polarization state in the cavity, the pump level and the gain profile. For instance, the laser starts radiating at 1981.1 nm and creates standing wave in the cavity. Accordingly, the anti-nodes of the initial created standing wave experiencing a more intensive population inversion depletion, while population inversion at nodes is less depleted, this leads to the lost of initial oscillating mode in the competition then the laser wavelength jumps to the next longitudinal mode. The above process caused by SHB keeps affecting the new selected oscillating frequency leads to wavelength sweeping to a determined direction as long as the gain is above the threshold. When the output wavelength decrease to its shortest wavelength, in other words, following the reverse sweeping direction (periodically from long wavelength to short), it bounces back to initial position and start over again. The wavelength range of the sweeping depends on the gain/loss spectral in the cavity, if there is no extra bandwidth limitation factor inside the cavity. Furthermore, the sweeping direction is decided even before the wavelength sweeping starts. The main effect that determines the sweeping direction is still under discussion. The effect of spectral gain profile was discussed in [73, 79, 12], besides, reference [79, 12] assumed that the normal (short wavelength to long wavelength) in Figure 5.9a and reverse (long wavelength to short wavelength) in Figure 5.9b sweeping

is determined by different effects, respectively. In the case of reverse sweeping direction, the radiating always starts at the longitudinal mode with maximum gain, the gain of shorter wavelength declines gradually since the absolute value of the gain derivative is smaller at the side of shorter wavelength in the gain contour. The physical mechanism are decipted in Fig 5.8 and Fig 5.9. The detial of this dynamic effect in one round trip can be explained as follow: firstly, cavity gain dynamic per round-trip-sinc hole is burned into the gain curve in global maximum position; then the hole glides along the gain curve in the direction of higher -sinc lobe gain; afterwards, as the former gain maximum becomes the global maximum again, the hole is "quenched" and a new one is created near the original one, which is also match with the edge shape of the wavelength output in Fig 5.2.

Since the output wavelength is unstable, the temporal output of a self-sweeping fiber laser is like Fig. 5.3a, which is a typical random pulse train of sustained relaxation oscillations. The high frequency modulation details of the pulse train is shown in Fig. 5.3b. The microsecond self-formed random pulses in Fig. 5.3a are caused by the relaxation oscillations with a modulation frequency resulting from the intermode beating frequency as shown in Fig.5.3b. The average pulse period of sustained relaxation is around 14 microseconds. The oscillating frequency caused by relaxation is determinded by the pump level and photon lifetime. The result is in agreement with other articles which reported several years ago.

It is worth to note that the self-sweeping regime can transfer into quasi-CW mode with the change of polarization states in the cavity. By tuning the paddle of polarization controller, the chaotic pulses formation in temporal and wavelength self-sweeping output can be elimated, and the new temporal characteristics indicating a self ampulitude modulation signal with a frequency related to relaxation oscillations in Fig 5.4a, the details of the ampulitude modulation signal is shown in Fig. 5.4b. The modulation index of CW direction is 38% and CCW direction has a modulation index about 28%. Under this quasi-stable temporal condition, the wavelength sweeping is diminished which is not surprising. Because once the counter-circulating wave are gradual Orthogonally by fixing the polarization state. So actually we can control the angle between propagating wave and fast axis, the sweepign rate variation can be controllable. It also reveals that when the laser reaches at the "quasi-stable" regime, the ratio of CCW and CW direction is around 0.5, indicating the unblanced gain in the cavity. The period of the stable ampulitude modulation signal is 14 microseconds similiar as the chaotic pulses in Fig. 5.3a. The modulation frequency in this regime is still representing the intermode beating frequency. We also record the results when we increase the pump power, Fig. 5.5a, Fig. 5.5b, Fig. 5.6a and Fig 5.6b shows the temporal characteristics of the self pulse formation with a higher pump level, the details of Fig. 5.5a, the temporal characteristics of the stable output with a higher pump level, the details of Fig. 5.6a, respectively. The

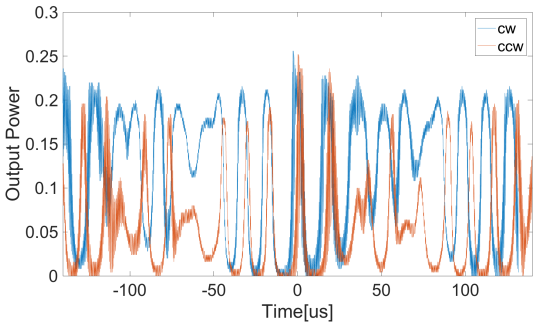

(a) Temporal characteristics of the laser output.

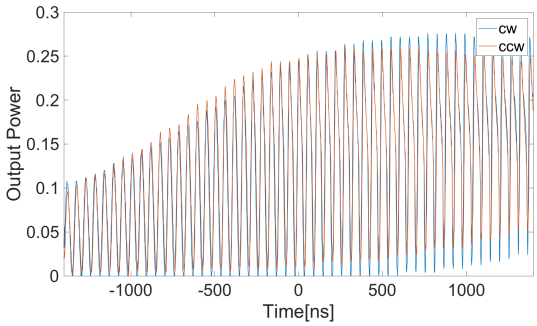

(b) Details of the microsecond pulse

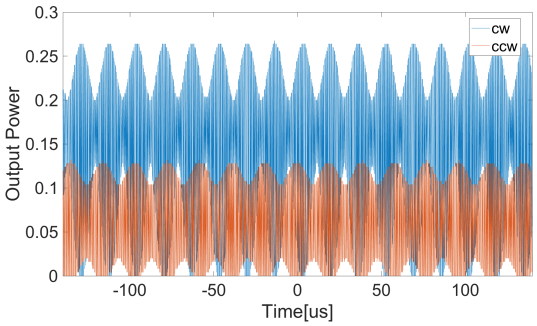

(a) Temporal characteristics of the laser stable output without chaotic self-formed pulses.

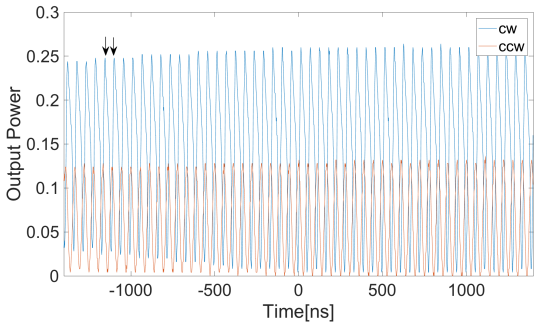

(b) Temporal characteristics of the laser stable output without chaotic self-formed pulses

stable ampulitude modulation regime can switch to random self-pulse regime by tuning the polarization controller. Furthermore, the higher pump level leads to more violent oscillations in self-pulse regime resulting in 10 microsecond period in temporal while the result in lower pump condition is 14 microsecond as we mentioned in previous paragraph. The difference in oscillation frequency is attributed to the relaxation oscillation frequency, for a certain pump power, the relaxation oscillation frequency is deteced by the rf spectrum analyzer, the result is depicted in Fig 5.7.

In summary, the spontaneous laser line sweeping (SLLS) phenomenon is demonstrated in this chapter. Spatial hole burning (SHB) effect and parasitic relaxation oscillation are discussed under the simple ring isolation-free laser cavity. The physical mechanism on sweepign direction is discussed. Besides, it is easy to understand that the severe of the chaotic level is depend on the angle between counter-circulating light wave, if two opposite light waves are exactly orthogonal.

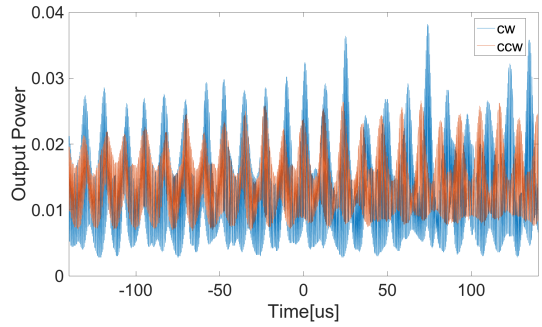

(a) Temporal characteristics of the laser with a higher pump power.

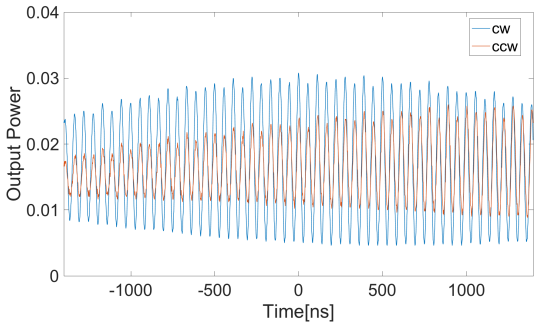

(b) Details of temporal characteristics of the laser with a higher pump power

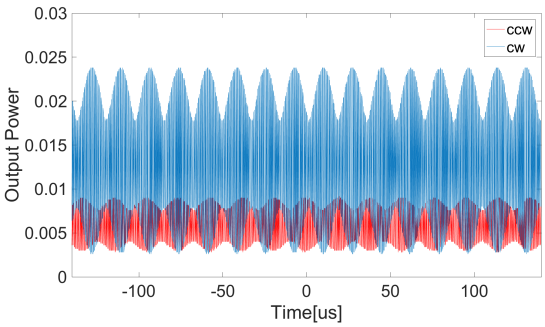

(a) Temporal characteristics of the laser stable output without chaotic self-formed pulses

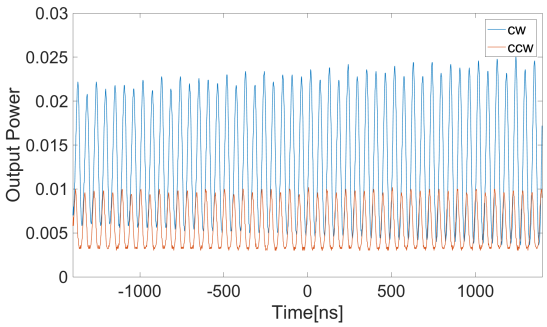

(b) Details of temporal characteristics of the laser with a higher pump power

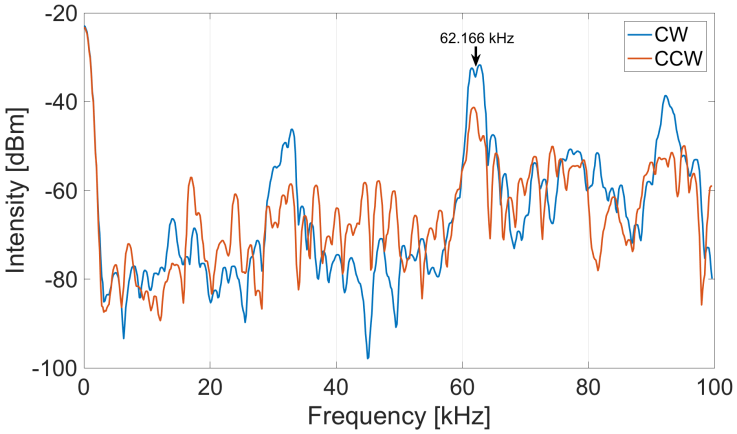

Fig. 5.7 Average frequency of relaxation oscillation

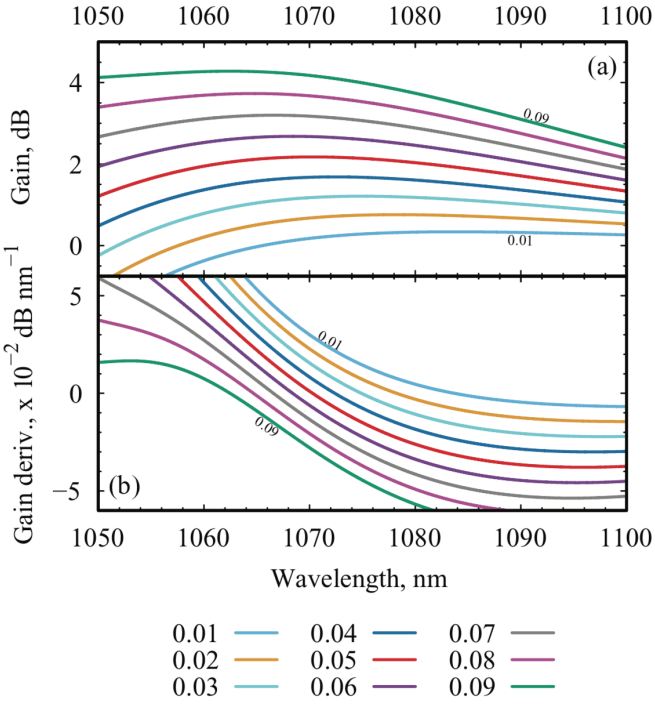

Fig. 5.8 Variation of cavity gain per round-trip spectra (a); spectra of the first derivative of the gain with respect to wavelength for different relative population inversion parameters (b) [12]

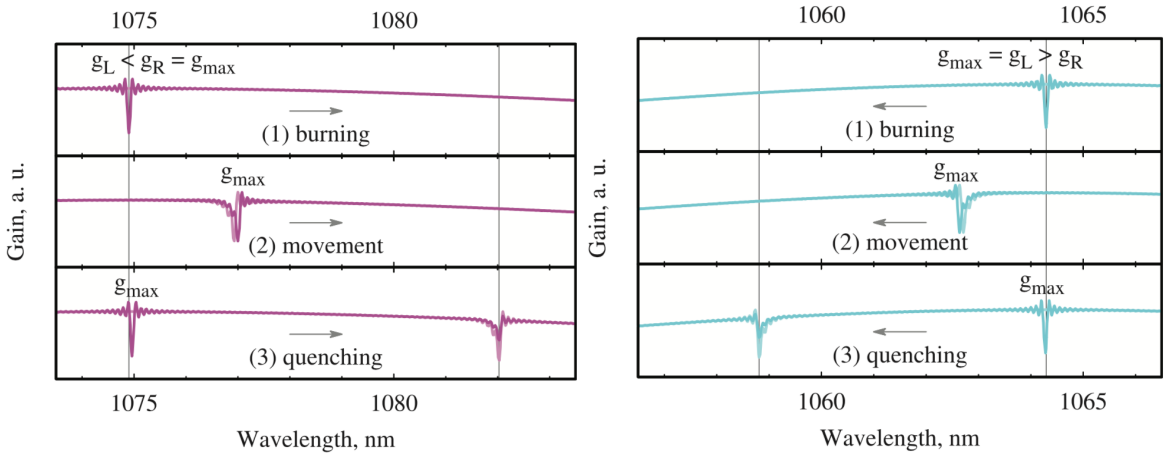

(a) normal sweeping.

(b) reverse sweeping.

Fig. 5.9 Cavity gain dynamic per round-trip. (1)-sinc hole is burned into the gain curve in global maximum position; (2) the hole glides along the gain curve in the direction of higher -sinc lobe gain; (3) as the former gain maximum becomes the global maximum again, the hole is "quenched" and a new one is created near the original one [12].

Chapter 6

Summary and Future Work

This chapter contains the summary of this thesis and an introduction on NPR typed passively mode locking method whose physical mechanism is not fully revealed. The principle of NPR and the defination of PDL are demonstrated firstly. Afterwards, the PDL induced mode locking is introduced with configuration and results from optical spectrum analyzer and digital oscilloscope. The future work on this mode locking method and isolator-free ring cavity laser are discussed as well.

6.1 Summary of the thesis

This thesis focuses on study of 2 μm isolation ring fiber laser with isolation-free structure, starts from fundamentals of mode locking theory including different mode locking methods, saturable absorber and common problems such as Q-switching, self-starting and multiple pulsing. Afterwards, the principle of optical frequency comb and spectroscopy techniques are introduced right behind the fundamentals of mode locking to emphasize the supremacy of mode locked laser as a comb source and purpose our ultimate goal of the experiment—to build a dual-comb spectroscopy with a isolator-free bi-directional mode-locked soliton fiber laser for carbon dioxide absorption measurement. However, we did not achieve the goal to make a stable dual-comb spectroscopy since the situation for stable output generation is difficult to control, which makes the generation of beating signal difficult unfortunately. We tried to manage the thesis focus on the analysis of the several factors that contributes to the separation of repetition rates such as group dispersion delay because of the difference in central wavelength, unbalanced configuration because of the reverse propagation experience, fiber birefringence contributes to the refractive index and Kerr-effect caused by the variation of intensity. The temporal- and frequency- domain results are depicted in chapter 4. Moreover, we found that the absence of optical isolator in the cavity result in strong positive feedback,

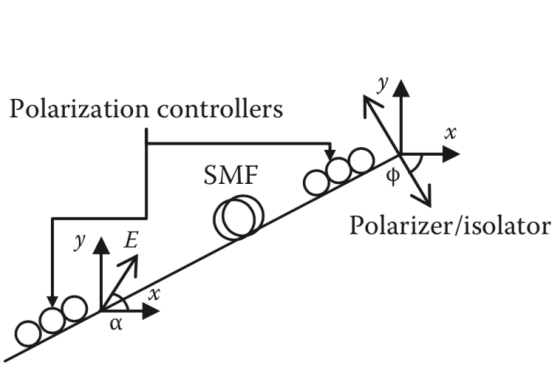

(a) Principle of the NPR technique.

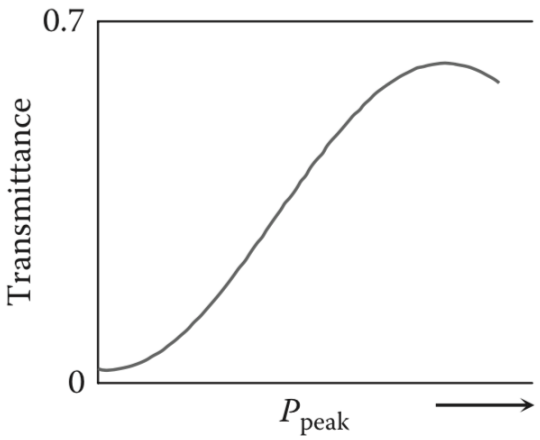

(b) Transmissivity of NPR.

Fig. 6.1 Description of operation and transmissivity of nonlinear polarization rotation [2].

which lead to spatial hole burning effect and parasitic relaxation oscillation in the medium. These phenomenon are categorized as laser longitudinal instability and these instabilities cause complex dynamic in the cavity, laser line self-sweeping in frequency and giant random pulse generation in time domain are depicted in detail, respectively. It is also worth to note that state of polarization in the cavity plays a key role for laser dynamic, one can accelerate or decline the sweeping rate even make still by only tuning the polarization controller. In other words, the creation of laser lines self-sweeping, or the creation of positive feedback induced standing wave, the angle of two counter-circulating light waves are important. This discovery can be extend to some sweeping source application and good paradigm for fiber laser longitudinal mode instability. Furthermore, a residual polarization dependent loss induced passive mode locking method is undergoing right now, the portion of observation results and possible physical mechanism is demonstrated in next section.

6.2 Nonlinear Polarization Rotation

Among the various passive mode locking techniques, NPR is the one that has been extensively investigated and widely used. Because of the all-fibered type, fast recovery time, variable saturable absorption strength, low cost the ease of implementation. Figure 6.1a shows a typical structure of NPR mode locking. The physical mechanism of NPR is the use of nonlinear birefringence. Conventionally, a polarizer or a polarization dependent isolator combined with two polarization controllers act as a mode locker as depicted. The function of polarizer make the light linearly polarized while the second polarization controller leads to

elliptical polarization. When a pulse propagating inside the mode locker, the polarization state evolves nonlinearly since two orthogonal polarization components in the birefringent fiber ring introduces the nonlinear phase shift. The transmission relationship is given by

$$T = cos^2\alpha cos^2\varphi + sin^2\alpha sin^2\varphi + \frac{1}{2}sin2\alpha sin2\phi cos(\Delta\phi_L + \Delta\phi_{NL}) \tag{6.1}$$

where α is the angle between the fast axis of fiber and the polarization direction of the input light, φ is the angel between the fast axis of fiber and the direction of polarizer, $\Delta\phi_L$ and $\Delta\phi_{NL}$ are linear and nonlinear phase bias between the two orthogonal polarization components which can be written as

$$\Delta\phi_L = \phi_L^y - \phi_L^x = \frac{2\pi L}{\lambda}(n_y - n_x) \tag{6.2}$$

$$\Delta\phi_{NL} = \phi_{NL}^y - \phi_{NL}^x = -\frac{\lambda LPcos2\alpha}{3} \tag{6.3}$$

Where n_y and n_x are the refractive indices of slow and fast axes of optical fiber, respectively. In more detail, $\Delta\phi_L$ is explained by the initial phase shift between the two orthogonal polarization modes and the inverse proportional factor of birefringence beat length while $\Delta\phi_{NL}$ is govern by the instantaneous power of the pulse so that the term T_{NPR} and peak power have a relationship as shown in Figure. 6.1b. In summary, if the transmission of the system increases with power, a positive regime is formed that allow NPR structure act like a saturable absorber.

So far almost every NPR mode locked fiber laser has a polarizer or at least an artificial component which has a large polarization dependent loss like tilted fiber grating polarization element [80–82] in the cavity. However we found that under strong pumping a fiber laser can mode lock even without the existence of a polarizer or other large polarization extinction ratio element in the cavity. The residual polarization dependent loss in the cavity and other potential physical mechanism are demonstrated in next section in detail. Since the experiment is still in progress so far, we just show the scheme of experiment setup and results from optical frequency analyzer and digital oscilloscope.

6.3 Mode Locking Results Analysis

The cavity configuration is shown in Fig 6.2. The cavity is constructed by fibers with anomalous dispersion in 1960 nm. It consists of 3 m thulium-doped fiber with group velocity

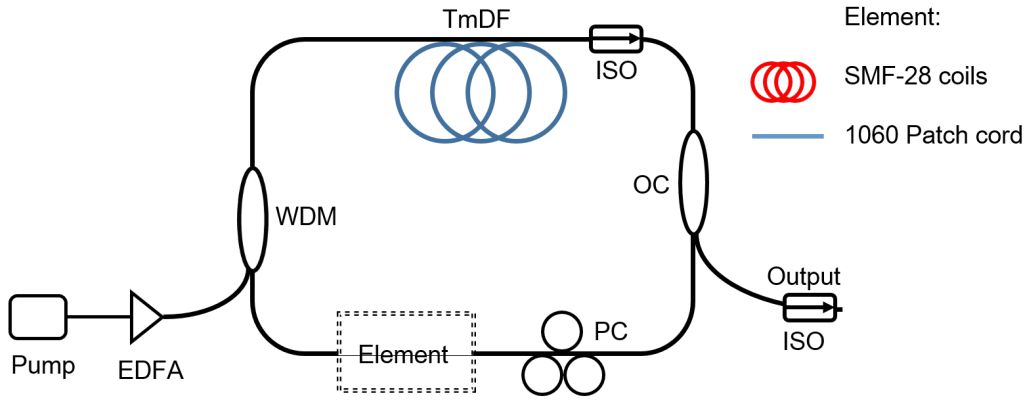

Fig. 6.2 Scheme of experiment setyp. WDM: wavelength division multiplexer; TmDF: thulium-doped fiber; OC: output coupler; ISO: optical isolator; PC: polarization controllers.

dispersion parameter of $-0.02ps^2/m$ in 1960 nm, and rest of fiber is SMF-28 with a group velocity dispersion parameter of $-0.06ps^2/m$ in 1960 nm. A polarization-independent optical isolator is inserted into the cavity to ensure the unidirectional operation of the laser. Only one polarization controller is inserted to tune the net cavity birefringence. The laser is pumped by a 1570 nm tunable laser which is amplified by an high power EDFA before pump through into a wavelength division multiplexer (WDM), and output coupler extract 30% output power from the cavity. We would like to emphasize again that different from the conventional NPR mode-locked fiber lasers, no polarizer or large polarization extinction ratio element is inserted into the cavity. The displacement of polarizer or large polarization extinction ratio element is fiber coils with a small radius consists of SMF-28 or a piece of patch cord with 1060 nm working wavelength. We believe the implementation of SMF-28 or a piece of patch core with 1060 nm working wavelength in a 2 micrometer fiber laser is the key element which enable the small but enough polarization dependent loss for NPR mode locking. We also believe the mode leaking mechanism in single mode fiber and the micro bending induced polarization dependent loss might not be the single reason for NPR mode locking in the fiber laser since we can achieve mode locking with a piece of patch cord with 1060 nm working wavelength without any man-made bending.

High pump power is required in this experiment, then the pump power is 220 mW, the fundamental soliton generation is achieved after carefully tuning the polarization controller. The optical spectra and pulse train from digital oscilloscope are depicted in Fig 6.3a and Fig 6.3b, respectively. The central wavelength of the spectra is 1913 nm since the bending loss is high in the micro bended fiber coils. The separation between pulses is about 10 MHz, which is corresponding to the length of the cavity. When the pump power raises to 277.1 mW, the separation between pulses corresponding to 15^{th} order of harmonic soliton generation

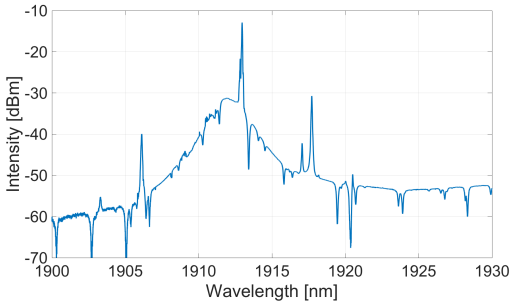

(a) Spectra of fundamental soliton.

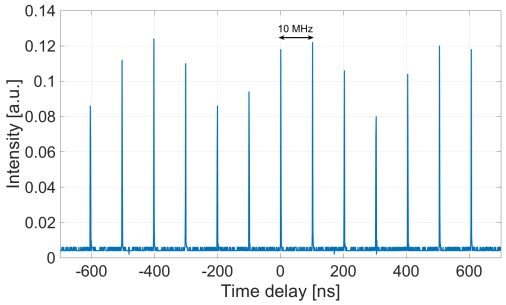

(b) Pulse train under fundamental mode

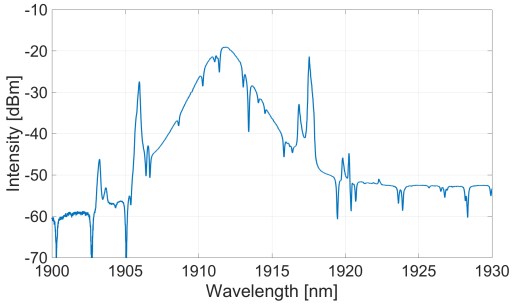

(a) Spectrum of 15^{th} generation.

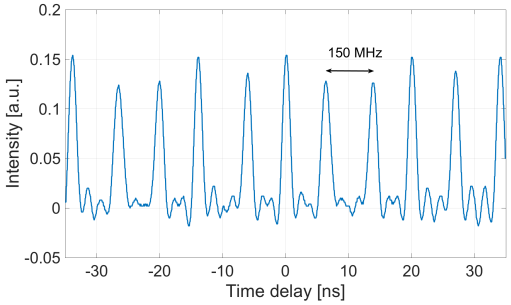

(b) Pulse train under 15^{th} harmonic

as shown in Fig 6.4b, which indicates that the laser output is unstable since there is a lot of sub-peaks exist between the output pulses. The spectra of harmonic output is depicted in Fig 6.4a and it has the similar central wavelength with fundamental soliton. Keeping elevating the pump level to 430 mW leads to the generation of harmonic pulses with a order larger the 40^{th}, the optical spectra and pulse train from digital oscilloscope are depicted in Fig 6.5a and Fig 6.5b, respectively. The separation between pulses corresponds to 400 MHz repetition rate, 40 times of the fundamental mode, the output peak becomes sin-like because the bandwidth of digital oscilloscope we used in the experiment is only 200 MHz.

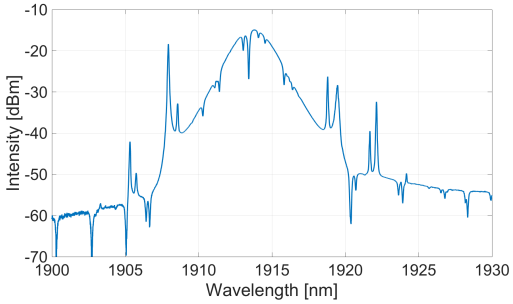

(a) Spectrum of 40^{th} generation.

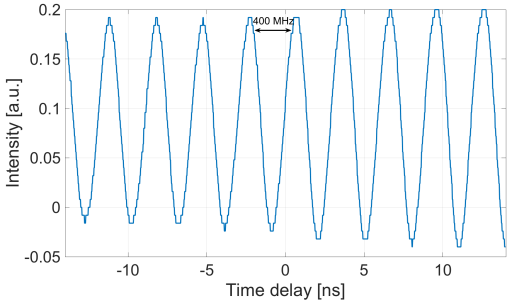

(b) Pulse train under 40^{th} harmonic

Table 6.1 Comparison among different experiment and corresponding polarization extinction ratio.

Mode Locker in the Laser	Maximum PDL	Dispersion Regime
45° tilted fiber grating [81]	33 dB	normal
45° tilted fiber grating [82]	30 dB	normal
45° tilted fiber grating [80]	20 dB	normal
45° tilted fiber grating [83]	20 dB	normal
Residual PDL induced by WDM [84]	3.1 dB	normal
Residual PDL induced by WDM [84]	1.2 dB	normal
Residual PDL induced by element 1	$<$ 1 dB	anomalous
Residual PDL induced by element 2	$<$ 1 dB	anomalous

When we replace the fiber coils of SMF-28 with a piece of patch cord with 1060 nm working wavelength, the similar result is confirmed. However, this time we can achieve mode locking without bending the fiber into small radius coils. We tried to measure the polarization dependent loss of element 1: fiber coils of SMF-28 with small radius and element 2: a piece of patch cord with 1060 nm working wavelength, the result is quite surprising that the PDL of these two elements is relatively small than we thought. The comparison among the different experiment is shown in table 6.1.

The comparison results indicates that the PDL required in anomalous dispersion regime is relatively small compared with the normal regime. Because of the lack of accurate PDL measurement in this experiment, the value of PDL induced by these two elements cannot be detected with a low uncertainty rate. The future work will be committed to the PDL detection and other potential physical mechanism in this 2 micrometer mode-locked fiber laser.

6.4 Future Work

Future on bi-directional soliton fiber laser will be focused on the stabilization control and generation of beating signal, the dual-comb spectroscopy setup, and the gas sample detection step by step. Besides, the application of spontaneous laser lines sweeping should be explored, and the physical mechanism of passive mode locking technique on residual PDL should be fully revealed as well.

References

[1] A. Weiner. *UltrafastOptics*. Welly, 2012.

[2] Dang Van Liet Le Nguyen Binh. *NONLINEAR OPTICAL SYSTEMS: Principles, Phenomena, and Advanced Signal Processing*. CRC Press, 2012.

[3] Birgitta Bernhardt. Dual comb spectroscopy. July 2011.

[4] Steven T. Cundiff Jun Ye. *Femtosecond Optical Frequency Comb: Principle, Operation and Applications*. Springer US, 2005.

[5] J. Mandon, G. Guelachvili, and N. Picqué. Fourier transform spectroscopy with a laser frequency comb. *Nature Photonics*, 3:99–102, February 2009.

[6] Birgitta Bernhardt, Akira Ozawa, Patrick Jacquet, Marion Jacquey, Yohei Kobayashi, Thomas Udem, Ronald Holzwarth, Guy Guelachvili, Theodor Haensch, and Nathalie Picqué. Cavity-enhanced dual-comb spectroscopy. 4:55–57, 01 2010.

[7] Alexandre Braga, Jean-Claude Diels, Ravinder Jain, Ronald Kay, and Li Wang. Bidirectional mode-locked fiber ring laser using self-regenerative, passively controlled, threshold gating. *Opt. Lett.*, 35(15):2648–2650, Aug 2010.

[8] Ahmet E. Akosman and Michelle Y. Sander. Dual comb generation from a mode-locked fiber laser with orthogonally polarized interlaced pulses. *Opt. Express*, 25(16):18592–18602, Aug 2017.

[9] Chunmei Ouyang, Ping Shum, Kan Wu, Jia Haur Wong, Huy Quoc Lam, and Sheel Aditya. Bidirectional passively mode-locked soliton fiber laser with a four-port circulator. *Opt. Lett.*, 36(11):2089–2091, Jun 2011.

[10] Khanh Kieu and Masud Mansuripur. All-fiber bidirectional passively mode-locked ring laser. *Opt. Lett.*, 33(1):64–66, Jan 2008.

[11] Yu Wang. Novel mode-locking techniques of tm-doped fiber lasers. July 2017.

[12] P Navratil, P Peterka, P Honzatko, and V Kubecek. Reverse spontaneous laser line sweeping in ytterbium fiber laser. *Laser Physics Letters*, 14(3):035102, 2017.

[13] Thomas F. Carruthers and Irl N. Duling. 10-ghz, 1.3-ps erbium fiber laser employing soliton pulse shortening. *Opt. Lett.*, 21(23):1927–1929, Dec 1996.

[14] M. Horowitz, E. C. Levy, O. Okusaga, C. R. Menyuk, W. Zhou, and G. M. Carter. Theoretical and experimental study of single and dual-loop optoelectronic oscillators. In *2009 IEEE International Conference on Microwaves, Communications, Antennas and Electronics Systems*, pages 1–3, 2009.

[15] S. Yang, J. Cameron, and X. Bao. Stabilized phase-modulated rational harmonic mode-locking soliton fiber laser. *IEEE Photonics Technology Letters*, 19(6):393–395, March 2007.

[16] C. R. Doerr, H. A. Haus, and E. P. Ippen. Asynchronous soliton mode locking. *Opt. Lett.*, 19(23):1958–1960, Dec 1994.

[17] Wei-Wei Hsiang, Chian-Yu Lin, Ming-Feng Tien, and Yinchieh Lai. Direct generation of a 10-ghz,81-fs pulse train from an erbium-fiber soliton laser with asynchronous phase modulation. *Opt. Lett.*, 30(18):2493–2495, Sep 2005.

[18] N. J. Doran and David Wood. Nonlinear-optical loop mirror. *Opt. Lett.*, 13(1):56–58, Jan 1988.

[19] M. E. Fermann, F. Haberl, M. Hofer, and H. Hochreiter. Nonlinear amplifying loop mirror. *Opt. Lett.*, 15(13):752–754, Jul 1990.

[20] Ursula Keller, Kurt J Weingarten, Franz X Kartner, Daniel Kopf, Bernd Braun, Isabella D Jung, Regula Fluck, Clemens Honninger, Nicolai Matuschek, and J Aus Der Au. Semiconductor saturable absorber mirrors (SESAM's) for femtosecond to nanosecond pulse generation in solid-state lasers. *IEEE Journal of selected topics in QUANTUM ELECTRONICS*, 2(3):435–453, 1996.

[21] Sze Y. Set, Hiroshi Yaguchi, Yuichi Tanaka, and Mark Jablonski. Laser mode locking using a saturable absorber incorporating carbon nanotubes. *J. Lightwave Technol.*, 22(1):51, Jan 2004.

[22] S. Yamashita, Y. Inoue, S. Maruyama, Y. Murakami, H. Yaguchi, M. Jablonski, and S. Y. Set. Saturable absorbers incorporating carbon nanotubes directly synthesized onto substrates and fibers and their application to mode-locked fiber lasers. *Opt. Lett.*, 29(14):1581–1583, Jul 2004.

[23] H. Zhang, D. Y. Tang, L. M. Zhao, Q. L. Bao, and K. P. Loh. Large energy mode locking of an erbium-doped fiber laser with atomic layer graphene. *Opt. Express*, 17(20):17630–17635, Sep 2009.

[24] H. Zhang, S. B. Lu, J. Zheng, J. Du, S. C. Wen, D. Y. Tang, and K. P. Loh. Molybdenum disulfide (mos2) as a broadband saturable absorber for ultra-fast photonics. *Opt. Express*, 22(6):7249–7260, Mar 2014.

[25] K. Tamura, E. P. Ippen, H. A. Haus, and L. E. Nelson. 77-fs pulse generation from a stretched-pulse mode-locked all-fiber ring laser. *Opt. Lett.*, 18(13):1080–1082, Jul 1993.

[26] Frithjof Haxsen, Axel Ruehl, Martin Engelbrecht, Dieter Wandt, Uwe Morgner, and Dietmar Kracht. Stretched-pulse operation of a thulium-doped fiber laser. *Opt. Express*, 16(25):20471–20476, Dec 2008.

[27] D. Popa, Z. Sun, F. Torrisi, T. Hasan, F. Wang, and A. C. Ferrari. Sub 200 fs pulse generation from a graphene mode-locked fiber laser. *Applied Physics Letters*, 97(20):203106, 2010.

[28] E. S. Boncristiano, L. A. M. Saito, and E. A. De Souza. 396 fs, 2.5-12 ghz asynchronous mode-locking erbium fiber laser. In *2007 Conference on Lasers and Electro-Optics (CLEO)*, pages 1–2, May 2007.

[29] K. R. Tamura and M. Nakazawa. 54-fs, 10-ghz soliton generation from a polarization-maintaining dispersion-flattened dispersion-decreasing fiber pulse compressor. *Opt. Lett.*, 26(11):762–764, Jun 2001.

[30] Shiquan Yang, Evgueni A. Ponomarev, and Xiaoyi Bao. Experimental study on relaxation oscillation in a detuned fm harmonic mode-locked er-doped fiber laser. *Optics Communications*, 245(1):371 – 376, 2005.

[31] Xiang Zhang, Hongyu Hu, Wenbo Li, and Niloy K. Dutta. High-repetition-rate ultrashort pulsed fiber ring laser using hybrid mode locking. *Appl. Opt.*, 55(28):7885–7891, Oct 2016.

[32] Bo Xu, Amos Martinez, Sze Yun Set, Chee Seong Goh, and Shinji Yamashita. A net normal dispersion all-fiber laser using a hybrid mode-locking mechanism. *Laser Physics Letters*, 11(2):025101, 2014.

[33] G. Agrawal. *Nonlinear Fiber Optics*. Welly, 2010.

[34] Y. Chen, F. X. Kärtner, U. Morgner, S. H. Cho, H. A. Haus, E. P. Ippen, and J. G. Fujimoto. Dispersion-managed mode locking. *J. Opt. Soc. Am. B*, 16(11):1999–2004, Nov 1999.

[35] Andy Chong, Joel Buckley, Will Renninger, and Frank Wise. All-normal-dispersion femtosecond fiber laser. *Opt. Express*, 14(21):10095–10100, Oct 2006.

[36] Andy Chong, William H. Renninger, and Frank W. Wise. Properties of normal-dispersion femtosecond fiber lasers. *J. Opt. Soc. Am. B*, 25(2):140–148, Feb 2008.

[37] H. Haus. Parameter ranges for cw passive mode locking. *IEEE Journal of Quantum Electronics*, 12(3):169–176, Mar 1976.

[38] C. Hönninger, R. Paschotta, F. Morier-Genoud, M. Moser, and U. Keller. Q-switching stability limits of continuous-wave passive mode locking. *J. Opt. Soc. Am. B*, 16(1):46–56, Jan 1999.

[39] Franz X. Kaertner. Control of solid state laser dynamics by semiconductor devices. *Optical Engineering*, 34:34 – 34 – 13, 1995.

[40] E. P. Ippen, L. Y. Liu, and H. A. Haus. Self-starting condition for additive-pulse mode-locked lasers. *Opt. Lett.*, 15(3):183–185, Feb 1990.

[41] H. A. Haus and E. P. Ippen. Self-starting of passively mode-locked lasers. *Opt. Lett.*, 16(17):1331–1333, Sep 1991.

[42] Ariel Gordon, Omri Gat, Baruch Fischer, and Franz X. Kärtner. Self-starting of passive mode locking. *Opt. Express*, 14(23):11142–11154, Nov 2006.

[43] D. Y. Tang, L. M. Zhao, B. Zhao, and A. Q. Liu. Mechanism of multisoliton formation and soliton energy quantization in passively mode-locked fiber lasers. *Phys. Rev. A*, 72:043816, Oct 2005.

[44] Steven T. Cundiff and Jun Ye. Colloquium: Femtosecond optical frequency combs. *Rev. Mod. Phys.*, 75:325–342, Mar 2003.

[45] Th. Udem, J. Reichert, R. Holzwarth, and T. W. Hänsch. Accurate measurement of large optical frequency differences with a mode-locked laser. *Opt. Lett.*, 24(13):881–883, Jul 1999.

[46] Th. Udem, J. Reichert, R. Holzwarth, and T. W. Hänsch. Absolute optical frequency measurement of the cesium d_1 line with a mode-locked laser. *Phys. Rev. Lett.*, 82:3568–3571, May 1999.

[47] Scott A. Diddams, David J. Jones, Long-Sheng Ma, Steven T. Cundiff, and John L. Hall. Optical frequency measurement across a 104-thz gap with a femtosecond laser frequency comb. *Opt. Lett.*, 25(3):186–188, Feb 2000.

[48] Steven T Cundiff. Phase stabilization of ultrashort optical pulses. *Journal of Physics D: Applied Physics*, 35(8):R43, 2002.

[49] H.R. Telle, G. Steinmeyer, A.E. Dunlop, J. Stenger, D.H. Sutter, and U. Keller. Carrier-envelope offset phase control: A novel concept for absolute optical frequency measurement and ultrashort pulse generation. *Applied Physics B*, 69(4):327–332, Oct 1999.

[50] Thomas Brabec and Ferenc Krausz. Intense few-cycle laser fields: Frontiers of nonlinear optics. *Rev. Mod. Phys.*, 72:545–591, Apr 2000.

[51] David J. Jones, Scott A. Diddams, Jinendra K. Ranka, Andrew Stentz, Robert S. Windeler, John L. Hall, and Steven T. Cundiff. Carrier-envelope phase control of femtosecond mode-locked lasers and direct optical frequency synthesis. *Science*, 288(5466):635–639, 2000.

[52] A. Apolonski, A. Poppe, G. Tempea, Ch. Spielmann, Th. Udem, R. Holzwarth, T. W. Hänsch, and F. Krausz. Controlling the phase evolution of few-cycle light pulses. *Phys. Rev. Lett.*, 85:740–743, Jul 2000.

[53] M. Niering, R. Holzwarth, J. Reichert, P. Pokasov, Th. Udem, M. Weitz, T. W. Hänsch, P. Lemonde, G. Santarelli, M. Abgrall, P. Laurent, C. Salomon, and A. Clairon. Measurement of the hydrogen 1*S*- 2*S* transition frequency by phase coherent comparison with a microwave cesium fountain clock. *Phys. Rev. Lett.*, 84:5496–5499, Jun 2000.

[54] S. A. Diddams, Th. Udem, J. C. Bergquist, E. A. Curtis, R. E. Drullinger, L. Hollberg, W. M. Itano, W. D. Lee, C. W. Oates, K. R. Vogel, and D. J. Wineland. An optical clock based on a single trapped 199hg+ ion. *Science*, 293(5531):825–828, 2001.

[55] Savely G. Karshenboim. Laser spectroscopy of simple atoms and precision tests of bound state QED. *Laser Phys.*, 11:1083–1087, 2001.

[56] A. A. Michelson and E. W. Morley. On the relative motion of the earth and the luminiferous ether. *American Journal of Science*, Series 3 Vol. 34(203):333–345, 1887.

[57] Seok-Jeong Lee, Bambang Widiyatmoko, Motonobu Kourogi, and Motoichi Ohtsu. Ultrahigh scanning speed optical coherence tomography using optical frequency comb generators. *Japanese Journal of Applied Physics*, 40(8B):L878, 2001.

[58] S. Schiller. Spectrometry with frequency combs. *Opt. Lett.*, 27(9):766–768, May 2002.

[59] Ian Coddington, William C. Swann, and Nathan R. Newbury. Coherent multiheterodyne spectroscopy using stabilized optical frequency combs. *Phys. Rev. Lett.*, 100:013902, Jan 2008.

[60] V. J. Matsas, T. P. Newson, D. J. Richardson, and D. N. Payne. Selfstarting passively mode-locked fibre ring soliton laser exploiting nonlinear polarisation rotation. *Electronics Letters*, 28(15):1391–1393, July 1992.

[61] J. Chesnoy. Picosecond gyrolaser. *Opt. Lett.*, 14(18):990–992, Sep 1989.

[62] Sho Okubo, Kana Iwakuni, Hajime Inaba, Kazumoto Hosaka, Atsushi Onae, Hiroyuki Sasada, and Feng-Lei Hong. Ultra-broadband dual-comb spectroscopy across 1.0–1.9 μm. *Applied Physics Express*, 8(8):082402, 2015.

[63] N. Buholz and M. Chodorow. Acoustic wave amplitude modulation of a multimore ring laser. *IEEE Journal of Quantum Electronics*, 3(6):235–235, June 1967.

[64] Khanh Kieu and Masud Mansuripur. Femtosecond laser pulse generation with a fiber taper embedded in carbon nanotube/polymer composite. *Opt. Lett.*, 32(15):2242–2244, Aug 2007.

[65] Venkatesh Mamidala, R. I. Woodward, Y. Yang, H. H. Liu, and K. K. Chow. Graphene-based passively mode-locked bidirectional fiber ring laser. *Opt. Express*, 22(4):4539–4546, Feb 2014.

[66] X. Zhao, Z. Zheng, Y. Liu, G. Hu, and J. Liu. Dual-wavelength, bidirectional single-wall carbon nanotube mode-locked fiber laser. *IEEE Photonics Technology Letters*, 26(17):1722–1725, Sept 2014.

[67] Maria Chernysheva, Mohammed Al Araimi, Hani Kbashi, Raz Arif, Sergey V. Sergeyev, and Aleksey Rozhin. Isolator-free switchable uni- and bidirectional hybrid mode-locked erbium-doped fiber laser. *Opt. Express*, 24(14):15721–15729, Jul 2016.

[68] Alexander A Krylov, Dmitry S Chernykh, and Elena D Obraztsova. Colliding-pulse hybridly mode-locked erbium-doped all-fiber soliton gyrolaser. *Laser Physics*, 28(1):015103, 2018.

[69] Yu Wang, Shaif ul Alam, Elena D. Obraztsova, Anatoly S. Pozharov, Sze Y. Set, and Shinji Yamashita. Generation of stretched pulses and dissipative solitons at 2 μm from an all-fiber mode-locked laser using carbon nanotube saturable absorbers. *Opt. Lett.*, 41(16):3864–3867, Aug 2016.

[70] Alexander A. Krylov, Dmitry S. Chernykh, and Elena D. Obraztsova. Gyroscopic effect detection in the colliding-pulse hybridly mode-locked erbium-doped all-fiber ring soliton laser. *Opt. Lett.*, 42(13):2439–2442, Jul 2017.

[71] Chao Zeng, Xueming Liu, and Ling Yun. Bidirectional fiber soliton laser mode-locked by single-wall carbon nanotubes. *Opt. Express*, 21(16):18937–18942, Aug 2013.

[72] Alexander A. Krylov, Dmitriy S. Chernykh, Natalia R. Arutyunyan, Vyacheslav V. Grebenyukov, Anatoly S. Pozharov, and Elena D. Obraztsova. Generation regimes of bidirectional hybridly mode-locked ultrashort pulse erbium-doped all-fiber ring laser with a distributed polarizer. *Appl. Opt.*, 55(15):4201–4209, May 2016.

[73] Ivan A. Lobach, Sergey I. Kablukov, Evgeniy V. Podivilov, and Sergey A. Babin. Broad-range self-sweeping of a narrow-line self-pulsing yb-doped fiber laser. *Opt. Express*, 19(18):17632–17640, Aug 2011.

[74] AVKiryanov and NNIichev. Self-induced laser line sweeping in an ytterbium fiber laser with non-resonant fabry-perot cavity. *Laser Physics Letters*, 8(4):305, 2011.

[75] P. Navratil, P. Peterka, P. Vojtisek, I. Kasik, J. Aubrecht, P. Honzatko, and V. Kubecek. Self swept erbium fiber laser. *Opto-Electronics Review*, 26(1):29 – 34, 2018.

[76] Xiong Wang, Pu Zhou, Xiaolin Wang, Hu Xiao, and Lei Si. Tm-ho co-doped all-fiber brand-range self-sweeping laser around 1.9 μm. *Opt. Express*, 21(14):16290–16295, Jul 2013.

[77] P. Peterka, P. Honzátko, P. Koška, F. Todorov, J. Aubrecht, O. Podrazký, and I. Kašík. Reflectivity of transient bragg reflection gratings in fiber laser with laser-wavelength self-sweeping. *Opt. Express*, 22(24):30024–30031, Dec 2014.

[78] Ivan A. Lobach, Sergey I. Kablukov, Mikhail A. Melkumov, Vladimir F. Khopin, Sergey A. Babin, and Evgeny M. Dianov. Single-frequency bismuth-doped fiber laser with quasi-continuous self-sweeping. *Opt. Express*, 23(19):24833–24842, Sep 2015.

[79] Jan Aubrecht, Pavel Peterka, Pavel Koška, Ondřej Podrazký, Filip Todorov, Pavel Honzátko, and Ivan Kašík. Self-swept holmium fiber laser near 2100 nm. *Opt. Express*, 25(4):4120–4125, Feb 2017.

[80] Chengbo Mou, Hua Wang, Brandon G. Bale, Kaiming Zhou, Lin Zhang, and Ian Bennion. All-fiber passively mode-locked femtosecond laser using a 45º-tilted fiber grating polarization element. *Opt. Express*, 18(18):18906–18911, Aug 2010.

[81] Xianglian Liu, Hushan Wang, Zhijun Yan, Yishan Wang, Wei Zhao, Wei Zhang, Lin Zhang, Zhi Yang, Xiaohong Hu, Xiaohui Li, Deyuan Shen, Cheng Li, and Guangde Chen. All-fiber normal-dispersion single-polarization passively mode-locked laser based on a 45°-tilted fiber grating. *Opt. Express*, 20(17):19000–19005, Aug 2012.

[82] Zuxing Zhang, Chengbo Mou, Zhijun Yan, Kaiming Zhou, Lin Zhang, and Sergei Turitsyn. Sub-100 fs mode-locked erbium-doped fiber laser using a 45°-tilted fiber grating. *Opt. Express*, 21(23):28297–28303, Nov 2013.

[83] Tianxing Wang, Zhijun Yan, Chengbo Mou, Zuyao Liu, Yunqi Liu, Kaiming Zhou, and Lin Zhang. Narrow bandwidth passively mode locked picosecond erbium doped fiber laser using a 45° tilted fiber grating device. *Opt. Express*, 25(14):16708–16714, Jul 2017.

[84] X. Wu, D. Y. Tang, L. M. Zhao, and H. Zhang. Mode-locking of fiber lasers induced by residual polarization dependent loss of cavity components. *Laser Physics*, 20(10):1913–1917, 2010.